7698 *Inorg. Chem.* **2009**, *48*, 7698–7713
DOI: 10.1021/ic9007069

Inorganic Chemistry
Article

Impact of Constitutional Isomers of ($BMes_2$)phenylpyridine on Structure, Stability, Phosphorescence, and Lewis Acidity of Mononuclear and Dinuclear Pt(II) Complexes

Ying-Li Rao and Suning Wang*

Department of Chemistry, Queen's University, Kingston, Ontario, K7L 3N6, Canada

Received April 10, 2009

The impact of two constitutional isomers, 2-(4-$BMes_2$-Ph)-pyridine (*p*-B-ppy, **1**) and 5-$BMes_2$-2-ph-pyridine (*p*-ppy-B, **2**), as N,C-chelate ligands on the structures, stabilities, electronic and photophysical properties, and Lewis acidities of Pt(II) complexes has been investigated. Six Pt(II) complexes, Pt(*p*-B-ppy)Ph(DMSO) (**1a**), Pt(*p*-B-ppy)Ph(py) (**1b**), [Pt(*p*-B-ppy)Ph]$_2$(4,4′-bipy) (**1c**), Pt(*p*-ppy-B)Ph(DMSO) (**2a**), Pt(*p*-ppy-B)Ph(py) (**2b**), and [Pt(*p*-ppy-B)Ph]$_2$(4,4′-bipy) (**2c**), have been synthesized and fully characterized. The structures of **1a**, **1c**, **2a**, and **2c** were established by single-crystal X-ray diffraction analysis. All complexes adopt a cis geometry with the phenyl ligand being cis to the phenyl ring of the ppy chelate. The dinuclear complexes **2a** and **2c** were found to exist in two isomeric forms in solution, syn and anti, with respect to the relative orientation of the two $BMes_2$ groups in the molecule. While all complexes are stable in solution under ambient air, compound **2a** was found to react with H_2O slowly in solution and form complex 2a−OH, where one of the mesityl groups on the boron center was replaced by an OH group. This instability of **2a** is attributed to an internal dimethylsulfoxide-directed hydrolysis process via hydrogen bonds. The electron-accepting ability of the free ligands and the complexes were examined by cyclic voltammetry, establishing that, for *p*-ppy-B, Pt(II) chelation enhances the electron-accepting ability while, for *p*-B-ppy, Pt(II) chelation has little impact. All Pt(II) complexes display oxygen-sensitive phosphorescence in solution at ambient temperature, dominated by B-ppy or ppy-B centered $\pi \rightarrow \pi^*$ transitions. The Lewis acidity of the complexes was examined by fluoride titration experiments using UV−vis, phosphorescence, and NMR spectroscopic methods, establishing that the *p*-ppy-B complexes have similar and strong binding constants while the *p*-B-ppy complexes have a much lower affinity toward F^-, compared to the free ligands. In the dinuclear complexes, weak electronic communication between the two Pt(II) units is evident in 1c but absent in **2c**, attributable to the different steric interactions in the two molecules.

Introduction

Conjugated triarylboron compounds are known to display unique photophysical and photochemical properties that have enabled their various applications, such as their use in emissive layers and charge-transport materials in organic light-emitting diodes (OLEDs),[1] nonlinear optics,[2] and anion sensors,[3,4] which can be attributed mostly to the p_π-to-π^* conjugation through the vacant p orbital on the boron center.

It has been reported recently that inclusion of a metal ion in the triarylboron compounds can lead to ambient temperature phosphorescence; high Lewis acidity; visual, electrochemical, and phosphorescent sensors for fluoride and cyanide ions; and so forth.[5,6] The synergic effect of metal-to-ligand charge transfer (MLCT) and π(aryl)-B charge transfer has been found to be responsible for many of the interesting properties of the metal-containing triarylboron complexes. On the basis of the binding modes, the majority of metal-containing triarylboron compounds reported to date belong to two categories: π complexes and σ complexes. The former has a metal center bound to a π donor such as a cyclopentadienyl

*To whom correspondence should be addressed. E-mail: wangs@chem.queensu.ca.

(1) (a) Noda, T.; Shirota, Y. *J. Am. Chem. Soc.* **1998**, *120*, 9714. (b) Shirota, Y. *J. Mater. Chem.* **2005**, *15*, 75. (c) Noda, T.; Ogawa, H.; Shirota, Y. *Adv. Mater.* **1999**, *11*, 283. (d) Shirota, Y.; Kinoshita, M.; Noda, T.; Okumoto, K.; Ohara, T. *J. Am. Chem. Soc.* **2000**, *122*, 1102. (e) Jia, W. L.; Bai, D. R.; McCormick, T.; Liu, Q. D.; Motala, M.; Wang, R.; Seward, C.; Tao, Y.; Wang, S. *Chem.—Eur. J.* **2004**, *10*, 994. (f) Jia, W. L.; Moran, M. J.; Yuan, Y. Y.; Lu, Z. H.; Wang, S. *J. Mater. Chem.* **2005**, *15*, 3326. (g) Jia, W. L.; Feng, X. D.; Bai, D. R.; Lu, Z. H.; Wang, S.; Vamvounis, G. *Chem. Mater.* **2005**, *17*, 164. (h) Li, F. H.; Jia, W. L.; Wang, S.; Zhao, Y. Q.; Lu, Z. H. *J. Appl. Phys.* **2008**, *103*, 034509/1–034509/6. (i) Wakamiya, A.; Mori, K.; Yamaguchi, S. *Angew. Chem., Int. Ed.* **2007**, *46*, 4237.

(2) (a) Collings, J. C.; Poon, S. Y.; Droumaguet, C. L.; Charlot, M.; Katan, C.; Pålsson, L. O.; Beeby, A.; Msely, J. A.; Kaiser, H. M.; Kaufmann, D.; Wong, W. Y.; Blanchard-Desce, M.; Marder, T. B. *Chem.—Eur. J.* **2009**, *15*, 198. (b) Yuan, Z.; Taylor, N. J.; Ramachandran, R.; Marder, T. B. *Appl. Organomet. Chem.* **1996**, *10*, 305. (c) Yuan, Z.; Entwistle, C. D.; Collings, J. C.; Albesa-Jové, D.; Batsanov, A. S.; Howard, J. A. K.; Kaiser, H. M.; Kaufmann, D. E.; Poon, S.-Y.; Wong, W. Y.; Jardin, C.; Fathallah, S.; Boucekkine, A.; Halet, J. F.; Taylor, N. J.; Marder, T. B. *Chem.—Eur. J.* **2006**, *12*, 2758. (d) Entwistle, C. D.; Marder, T. B. *Angew. Chem., Int. Ed.* **2002**, *41*, 2927. (e) Entwistle, C. D.; Marder, T. B. *Chem. Mater.* **2004**, *16*, 4574. (f) Stahl, R.; Lambert, C.; Kaiser, C.; Wortmann, R.; Jakober, R. *Chem.—Eur. J.* **2006**, *12*, 2358. (g) Matsumi, N.; Chujo, Y. *Polym. J.* **2008**, *40*, 77. (h) Lequan, M.; Lequan, R. M.; Ching, K. C. *J. Mater. Chem.* **1991**, *1*, 997. (i) Liu, Z. Q.; Fang, Q.; Cao, D. X.; Wang, D.; Xu, G. B. *Org. Lett.* **2004**, *6*, 2933. (j) Tao, L. M.; Guo, Y. H.; Huang, X. M.; Wang, C. K. *Chem. Phys. Lett.* **2006**, *425*, 10.

Published on Web 07/21/2009

anion that is functionalized by a triarylboron center,[6] while the latter contains a metal ion that is bound to a σ donor such as 2,2′-bipy with a conjugated triarylboron group.[5] Among the σ complexes, in addition to *N*,*N*-chelate ligands,[1e,5a−c] *N*,*C*-chelate complexes based on phenylpyridine (ppy)[5d−f] or *N*-(2-py)-7-azaindole (NPA)[5g] functionalized by a $BMes_2$ (Mes = mesityl) group have been reported. The ppy chelate chromophore and its derivatives are most effective in producing highly emissive Ir(III) phosphorescent compounds.[5d−f] Several Ir(III) complexes based on $BMes_2$-functionalized ppy (*p*-B-ppy, *m*-B-ppy) and the closely related 2-(*p*-$BMes_2$-phenyl)-quinoline (*p*-B-pq) molecule (Chart 1) have been reported recently and used successfully either as a phosphorescent emitter in OLEDs or as a sensor for fluoride ions.[5d−f] Notably, these previously reported ppy derivatives all have the $BMes_2$ group at the phenyl ring, instead of the pyridyl or quinoline ring, perhaps due to the relatively easy functionalization of the phenyl ring, compared to the pyridyl or quinoline ring. We have reported recently that the direct attachment of a $BMes_2$ group to a pyridyl ring (e.g., 2,2-bipy) can greatly enhance its Lewis acidity.[5b,c] Hence, the B-ppy constitutional isomers with a $BMes_2$ group attached on the pyridyl ring, such as *p*-ppy-B shown in Chart 1, are worthy candidates for investigation. On the basis of this consideration, we have synthesized *p*-ppy-B and compared its properties to those of *p*-B-ppy. To examine the impact of the isomers of *p*-B-ppy and *p*-ppy-B on the properties of the metal complexes, we also synthesized a series of *N*,*C*-chelate Pt(II) complexes based on these two ligands.

Chart 1

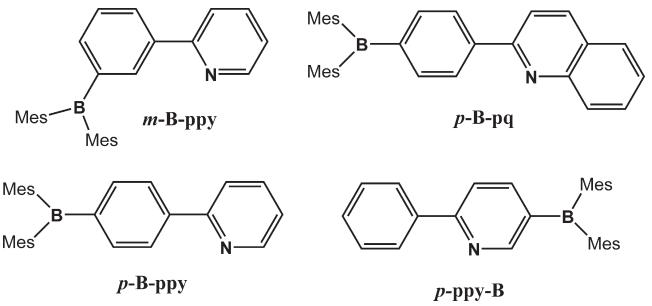

Pt(II) complexes are chosen because of their many potential applications such as vapochromic materials,[7] photochemical materials that convert light to chemical energy,[8] and emissive dopants in OLEDs.[9] Unlike *N*,*N*-chelate Pt(II) complexes of polypyridine ligands[10] that display phosphorescence dominated by MLCT transition mixed with ^{3}LC (ligand-centered) transitions, *N*,*C*-chelate Pt(II) complexes based on ppy and derivative ligands are known to display mostly ^{3}LC phosphorescence.[9a] Thus, the inclusion of the $BMes_2$ group on the ppy ligand would allow the direct observation of its impact on MLCT transitions and the possible enhancement of MLCT phosphorescence. To facilitate our investigation, Pt(II) complexes with different ancillary ligands such as DMSO and pyridine were prepared and examined. In addition, to examine the impact of the *p*-B-ppy and *p*-ppy-B ligands on possible electronic communication between two boron centers via a conjugated Pt_2 unit, dinuclear Pt(II) complexes with 4,4-bipyridine as the bridging/ancillary ligand were also prepared and investigated. The anion binding ability of the new Pt(II) complexes was studied through UV−vis, phosphorescence, and NMR spectroscopic methods. The results of this comprehensive study are reported herein.

Experimental Section

All reactions were performed under N_2 with standard Schlenk techniques unless otherwise noted. All starting materials were purchased from Aldrich Chemical Company and used without further purification. DMF, THF, Et_2O, and hexanes were purified using an Innovation Technology Company solvent purification system. CH_2Cl_2 was freshly distilled over P_2O_5 prior to use. NMR spectra were recorded on Bruker Avance 400 or 500 MHz spectrometers. High-resolution mass spectra were obtained from a Waters/Micromass GC-TOF EI-MS spectrometer. Cyclic voltammetry was performed using a BAS CV-50W analyzer with a scan rate of 100 mV/s to 1 V/s and a typical concentration of ~0.003 M in DMF using 0.10 M tetrabutylammonium hexafluorophosphate (TBAP) as the supporting electrolyte. A conventional three-compartment electrolytic cell consisting of a Pt working

(3) (a) Yamaguchi, S.; Shirasaka, T.; Akiyama, S.; Tamao, K. *J. Am. Chem. Soc.* **2002**, *124*, 8816. (b) Yamaguchi, S.; Akiyama, S.; Tamao, K. *J. Am. Chem. Soc.* **2001**, *123*, 11372. (c) Solé, S.; Gabba, F. P. *Chem. Commun.* **2004**, 1284. (d) Melaimi, M.; Gabba, F. P. *J. Am. Chem. Soc.* **2005**, *127*, 9680. (e) Chiu, C. W.; Gabba, F. P. *J. Am. Chem. Soc.* **2006**, *128*, 14248. (f) Hudnall, T. W.; Melaimi, M.; Gabba, F. P. *Org. Lett.* **2006**, *8*, 2747. (g) Lee, M. H.; Agou, T.; Kobayashi, J.; Kawashima, T.; Gabba, F. P. *Chem. Commun.* **2007**, 1133. (h) Lee, M. H.; Gabba, F. P. *Inorg. Chem.* **2007**, *46*, 8132. (i) Hudnall, T. W.; Gabba, F. P. *J. Am. Chem. Soc.* **2007**, *129*, 11978. (j) Dorsey, C. L.; Jewula, P.; Hudnall, T. W.; Hoefelmeyer, J. D.; Taylor, T. J.; Honesty, N. R.; Chiu, C.-W.; Schulte, M.; Gabba, F. P. *Dalton Trans.* **2008**, 4442. (k) Hudnall, T. W.; Kim, Y.-M.; Bebbington, M. W. P.; Bourissou, D.; Gabba, F. P. *J. Am. Chem. Soc.* **2008**, *130*, 10890.

(4) (a) Sundararaman, A.; Venkatasubbaiah, K.; Victor, M.; Zakharov, L. N.; Rheingold, A. L.; Jäkle, F. *J. Am. Chem. Soc.* **2006**, *128*, 16554. (b) Parab, K.; Venkatasubbaiah, K.; Jäkle, F. *J. Am. Chem. Soc.* **2006**, *128*, 12879. (c) Jäkle, F. *Coord. Chem. Rev.* **2006**, *250*, 1107. (d) Liu, X. Y.; Bai, D. R.; Wang, S. *Angew. Chem., Int. Ed.* **2006**, *45*, 5475. (e) Bai, D. R.; Liu, X. Y.; Wang, S. *Chem.—Eur. J.* **2007**, *13*, 5713. (f) Zhao, S. B.; Wucher, P.; Hudson, Z. M.; McCormick, T. M.; Liu, X. Y.; Wang, S.; Feng, X. D.; Lu, Z. H. *Organometallics* **2008**, *27*, 6446. (g) Zhou, G.; Baumgarten, M.; Müllen, K. *J. Am. Chem. Soc.* **2008**, *130*, 12477.

(5) (a) Sakuda, E.; Funahashi, A.; Kitamura, N. *Inorg. Chem.* **2006**, *45*, 10670. (b) Sun, Y.; Ross, N.; Zhao, S. B.; Huszarik, K.; Jia, W. L.; Wang, R. Y.; Wang, S. *J. Am. Chem. Soc.* **2007**, *129*, 7510. (c) Sun, Y.; Wang, S. *Inorg. Chem.* **2009**, *48*, 3755. (d) Zhou, G. J.; Ho, C. L.; Wong, W. Y.; Wang, Q.; Ma, D. G.; Wang, L. X.; Lin, Z. Y.; Marder, T. B.; Beeby, A. *Adv. Funct. Mater.* **2008**, *18*, 499. (e) You, Y. M.; Park, S. Y. *Adv. Mater.* **2008**, *20*, 3820. (f) Zhao, Q.; Li, F. Y.; Liu, S. J.; Yu, M. X.; Liu, Z. Q.; Yi, T.; Huang, C. H. *Inorg. Chem.* **2008**, *47*, 9256. (g) Zhao, S. B.; McCormick, T.; Wang, S. *Inorg. Chem.* **2007**, *46*, 10965. (h) Hudson, Z. M.; Zhao, S. B.; Wang, S. *Chem.—Eur. J.* **2009**, in press.

(6) For recent examples, see: (a) Venkatasubbaiah, K.; Nowik, I.; Herber, R. H.; Jäkle, F. *Chem. Commun.* **2007**, 2154. (b) Venkatasubbaiah, K.; Pakkirisamy, T.; Lalancette, R. A.; Jäkle, F. *Dalton Trans.* **2008**, 4507. (c) Broomsgrove; Alexander, E. J.; Addy, D. A.; Bresner, C.; Fallis, I. A.; Thompson, A. L.; Aldridge, S. *Chem.—Eur. J.* **2008**, *14*, 7525. (d) Day, J. K.; Bresner, C.; Coombs, N. D.; Fallis, I. A.; Ooi, L. L.; Aldridge, S. *Inorg. Chem.* **2008**, *47*, 793.

(7) (a) Kunugi, Y.; Mann, K. R.; Miller, L. L; Extrom, C. L. *J. Am. Chem. Soc.* **1998**, *120*, 589. (b) Kui, S.; Chui, S.; Che, C.; Zhu, N. *J. Am. Chem. Soc.* **2006**, *128*, 8297. (c) Zhao, Q.; Li, L.; Li, F.; Yu, M.; Liu, Z.; Yi, T.; Huang, C. *Chem. Commun.* **2008**, 685.

(8) (a) Hissler, M.; McGarrah, J. E.; Connick, W. B.; Geiger, D. K.; Cummings, S. D.; Eisenberg, R. *Coord. Chem. Rev.* **2000**, *208*, 115. (b) McGarrah, J. E.; Kim, Y.-J.; Hissler, M.; Eisenberg, R. *Inorg. Chem.* **2001**, *40*, 4510.

(9) (a) Brooks, J.; Babayan, Y.; Lamansky, S.; Djurovich, P.; Tsyba, I.; Bau, R.; Tompson, M. E. *Inorg. Chem.* **2002**, *41*, 3055. (b) Adamovich, V.; Brooks, J.; Tamayo, A.; Alexander, A. M.; Djurovich, P. I.; D'Andrade, B. W.; Adachi, C.; Forrest, S. R.; Tompson, M. E. *New J. Chem.* **2002**, *26*, 1171. (c) Lu, W.; Mi, B. X.; Chan, M. C. W.; Hui, Z.; Che, C. M.; Zhu, N.; Lee, S. T. *J. Am. Chem. Soc.* **2004**, *126*, 4958.

(10) (a) McMillin, D. R.; Moore, J. *Coord. Chem. Rev.* **2002**, *229*, 113. (b) McGarrah, J. E.; Eisenberg, R. *Inorg. Chem.* **2003**, *42*, 4355. (c) Yam, V. W.; Chan, K. H.; Wong, K. M.; Chu, B. W. *Angew. Chem., Int. Ed.* **2006**, *45*, 6169.

electrode, a Pt auxiliary electrode, and a Ag/AgCl reference electrode was employed using the ferrocene/ferrocenium couple as the standard ($E_{1/2} = 0.55$ V in DMF). UV−vis spectra were recorded on an Ocean Optics UV−visible spectrometer. Excitation and emission spectra were recorded on a Photon Technologies International QuantaMaster model C-60 spectrometer. Emission lifetimes were measured on a Photon Technologies International Phosphorimeter (TimeMaster C-631F) equipped with a xenon flash lamp and digital emission photon multiplier tube using a band pathway of 5 nm for excitation and 2 nm for emission. $[PtPh_2(DMSO)_2]$ was synthesized according to a previous report.[11]

Synthesis of 2-(4-Bromophenyl)-Pyridine. 2-(4-Bromophenyl)-pyridine is a previously known compound.[12] The procedure described here for this molecule is different from the previously reported one. To a stirred THF (30 mL) solution of 1 4-dibromobezene (4 g, 16.9 mol) at −78 °C was added dropwise an *n*-BuLi solution (1.6 M; 11.6 mL, 18.6 mol) over 2 min. The resulting solution with white precipitates was stirred for 1 h at −78 °C, and a $B(OMe)_3$ solution (30 mmol, 3.3 mL) was then added. After stirring at −78 °C for 1 h, the resulting transparent solution was warmed to ambient temperature and stirred overnight. A saturated NH_4Cl solution (20 mL) was added. After extraction of the aqueous layer with Et_2O (2 × 30 mL), the organic layer was dried with Na_2SO_4. After removal of the solvent, the residual 4-bromo-phenylboronic acid was used in next step without further purification. A mixture of toluene (60 mL), ethanol (20 mL), and water (20 mL) was stirred and purged by nitrogen for 1 h. 2-Bromopyridine (1.58 g, 10 mmol), 4-bromophenylboronic acid (2.00 g, 10 mmol), $Pd(PPh_3)_4$ (0.31 g, 0.25 mmol), and NaOH (2.5 g, 62.5 mmol) were added to the mixed solvents. The mixture was stirred at room temperature for 2 days. The aqueous layer was separated and extracted with CH_2Cl_2 (3 × 30 mL). The combined organic layers were dried over Na_2SO_4, and the solvents were evaporated under reduced pressure. Purification of the crude product by column chromatography (CH_2Cl_2/hexane, 1:1) afforded the product 2-(4-bromophenyl)-pyridine as a white solid in 51% yield (0.68 g).

Synthesis of 2-(4-BMes$_2$-Ph)-Pyridine (*p*-B-ppy, 1). To a stirred THF solution of 2-(4-bromophenyl)-pyridine (0.60 g, 2.3 mmol) at −78 °C was added dropwise an *n*-BuLi solution (1.60 M; 1.5 mL, 2.4 mmol) over 2 min. The resulting bright yellow solution was stirred for 1 h at −78 °C; a solution of dimesitylboron fluoride (0.75 g, 90%, 2.5 mmol) in Et_2O was then quickly added. The reaction mixture was kept at −78 °C for another 1 h and allowed to reach ambient temperature. After being stirred overnight and removal of the solvent, purification of the crude product by column chromatography (CH_2Cl_2/hexane, 2:1) afforded **1** as a white solid in 81% yield. ^{1}H NMR (400 MHz, $CDCl_3$, 25 °C, δ, ppm): 8.73 (d, $J = 6.0$ Hz; 1H), 8.99 (d, $J = 8.0$ Hz; 2H), 7.78 (m; 3H), 7.65 (d; $J = 8.4$ Hz; 2H), 7.26 (dd; 1H), 6.85 (s; 4H), 2.34 (s, 6H), 2.05 (s, 12H). ^{13}C{^{1}H}NMR (100 MHz, $CDCl_3$, δ, ppm): 157.53, 150.12, 146.78, 142.67, 142.06, 141.19, 139.05, 137.11, 137.05, 128.52, 126.73, 122.78, 121.32, 23.78, 21.55. HRMS calcd for $C_{29}H_{31}BN$ $[M]^+$: m/z 404.2549. Found: 404.2548.

Synthesis of 5-BMes$_2$-2-ph-Pyridine (*p*-ppy-B, 2). 3-Bromo-2-ph-pyridine is a previously known molecule.[13] The synthetic method we employed is different from the literature procedure, namely, via Suzuki coupling of phenylboronic acid and 2, 5-dibromopyridine at ambient temperature in a similar manner as described for the synthesis of 2-(4-bromophenyl)-pyridine. 5-BMes$_2$-2-Ph-pyridine was obtained by adding dimesitylboron fluoride after lithiation of 3-bromo-2-ph-pyridine in diethyl ether at −78 °C in the same manner as for the synthesis of **1**. Purification of the crude product by column chromatography (CH_2Cl_2/hexane, 1:1) afforded **2** as a white solid in 46% yield. ^{1}H NMR (400 MHz, $CDCl_3$, 25 °C, δ, ppm): 8.75 (s, 1H), 8.12 (d, $J = 7.2$ Hz; 2H), 7.84 (dd, $J = 8.0$ Hz, $J = 1.6$ Hz; 1H), 7.75 (d; $J = 8.0$ Hz; 1H), 7.48 (m; 3H), 6.86 (s; 4H), 2.33 (s, 6H), 2.06 (s, 12H). ^{13}C{^{1}H}NMR (100 MHz, $CDCl_3$, δ, ppm): 159.81, 157.51, 144.79, 141.06, 139.46, 139.25, 129.90, 129.10, 128.70, 127.50, 120.07, 116.91, 23.85, 21.53. HRMS calcd for $C_{29}H_{31}BN$ $[M]^+$: m/z 404.2549. Found: 404.2552.

Synthesis of Pt(*p*-B-ppy)Ph(DMSO), 1a. To a stirred THF (20 mL) solution of $[PtPh_2(DMSO)_2]$ (96 mg, 0.19 mmol) was added *p*-B-ppy (80 mg, 0.20 mmol). The mixture was stirred at 50 °C for 6 h, and the solvent was removed under reduced pressure. Yellow needle crystals of **1a** were obtained from hexane/CH_2Cl_2 (65% yield). ^{1}H NMR (500 MHz, CD_2Cl_2, 25 °C, δ, ppm): 8.69 (d, $J = 5.5$ Hz; 1H, py), 7.94 (m; 2H, py), 7.60 (d, $J = 7.5$ Hz; 1H, py), 7.28 (m; 4H, Ph), 6.75 (m; 8H), 2.91 (s; 6H, *Me*-DMSO), 2.34 (s, 6H, *p*-*Me*-Mes), 1.93 (s, 12H, *o*-*Me*-Mes). ^{13}C{^{1}H}NMR (100 MHz, CD_2Cl_2, δ, ppm): 165.16, 151.94, 151.85, 149.44, 146.62, 144.47, 140.56, 139.02, 138.34, 137.31, 133.22, 128.32, 128.08, 123.54, 122.82, 122.62, 119.87, 44.16, 23.43, 21.32. Anal. Calcd for $C_{37}H_{40}BNOPtS$: C, 59.04; H, 5.36; N, 1.86. Found: C, 59.15; H, 5.43; N, 1.92.

Synthesis of Pt(*p*-ppy-B)Ph(DMSO), 2a. To a stirred THF (20 mL) solution of $[PtPh_2(DMSO)_2]$ (96 mg, 0.19 mmol) was added 5-BMes$_2$-2-ph-py (80 mg, 0.20 mmol). The mixture was stirred at 50 °C for 6 h, and the solvent was removed under reduced pressure. Bright yellow needle crystals of **2a** were obtained from hexane/CH_2Cl_2 (60% yield) under nitrogen. ^{1}H NMR (500 MHz, CD_2Cl_2, 25 °C, δ, ppm): 9.57 (s; 1H, py), 7.94 (d, $J = 8.0$ Hz; 1H, py), 7.86 (d, $J = 8.0$ Hz; 1H, py), 7.71 (d, $J = 7.5$ Hz; 1H, *py*-Ph), 7.48 (d, satellite, $J = 8.0$ Hz, $J_{Pt-H} = 66.0$ Hz; 2H, *o*-ph), 7.09 (m; 3H, *py*-Ph), 7.01 (m; 2H, Ph), 6.90 (s; 4H, Mes), 6.68 (d, satellite, $J = 7.5$ Hz, $J_{Pt-H} = 65.0$ Hz; 1H, Ph), 2.72 (s; 6H, *Me*-DMSO), 2.35 (s; 6H, *o*-*Me*-Mes), 2.10 (s, 12 H, *p*-*Me*-Mes). ^{13}C{^{1}H}NMR (100 MHz, CD_2Cl_2, δ, ppm): 167.63, 159.15, 154.10, 146.34, 146.23, 146.06, 144.21, 139.83, 138.00, 137.84, 130.49, 128.77, 128.36, 125.24, 124.39, 123.19, 118.82, 44.07, 23.78, 21.37. Anal. Calcd for $C_{37}H_{40}BNOPtS$: C, 59.04; H, 5.36; N, 1.86. Found: C, 59.44; H, 5.83; N, 1.81. The hexane solvent molecule was removed by drying the sample under a vacuum.

Synthesis of PtPh[5-B(OH)(Mes)-2-Ph-py](DMSO), 2a−OH. To a THF solution (10 mL) of **2a** (20 mg, 0.027 mmol) was added 5 mL of toluene. The solution was kept under air, and the solvent was allowed to slowly evaporate at ambient temperature. Yellow crystals of **2a−OH** were obtained and isolated after ~20 days in ~70% yield. ^{1}H NMR (400 MHz, DMSO-d6, 25 °C, δ, ppm): 10.67 (s, 1H, B−OH), 9.83 (s; 1H, py), 8.06 (d, $J = 8.0$ Hz; 1H, py), 7.95 (d, $J = 8.0$ Hz; 1H, py), 7.77 (d, $J = 7.5$ Hz; 1H, ph), 7.38 (d, satellites, $J = 7.5$ Hz, $J_{Pt-H} = 65.0$ Hz; 2H, ph), 7.01 (m; 3H, ph, *Py*-ph), 6.89(m, 2H, *Py*-ph), 6.83 (s, 2H, Mes), 6.50 (d, satellites, $J = 8.0$ Hz, $J_{Pt-H} = 45.0$ Hz; 1H, *Py*-ph), 2.53 (s, 6H, Me-DMSO), 2.26 (s; 3H, *o*-Me-Mes), 2.13 (s, 6 H, *p*-Me-Mes). Anal. Calcd for $C_{28}H_{30}BO_2NPtS$: C, 51.70; H, 4.65; N, 2.15. Found: C, 50.87; H, 4.47; N, 2.08. (The toluene solvent molecules escaped from the crystal lattice at ambient temperature.)

Synthesis of Pt(*p*-B-ppy)Ph(py), 1b. To a CH_2Cl_2 (2 mL) solution of **1a** (20 mg, 0.027 mmol) was added pyridine (3 μL, 0.037 mmol). Yellow powders of **1b** were obtained after several hours of standing at ambient temperature (90% yield). ^{1}H NMR (500 MHz, CD_2Cl_2, 25 °C, δ, ppm): 8.86 (dd, $J = 7.2$ Hz, $J = 1.6$ Hz; 2H, py), 7.87 (m; 3H, py, *py*-Ph), 7.70 (d, $J = 5.2$ Hz; 1H, *py*-Ph), 7.56 (d; $J = 8.0$ Hz; 1H, B-*Ph*), 7.46 (td; $J = 6.0$ Hz, $J = 1.2$ Hz; 2H, py), 7.29 (s, satellites, $J_{Pt-H} = 45.0$ Hz; 1H, B-*Ph*), 7.25 (dd, satellites, $J = 8.0$ Hz, $J = 1.2$ Hz; 2H, ph), 7.14 (dd, $J = 7.6$ Hz, $J = 1.2$ Hz; 1H, B-*Ph*), 7.08 (td, $J = 7.6$ Hz, $J = 1.2$ Hz;

(11) Klein, A.; Schurr, T.; Knodler, A.; Gudat, D.; Klinkhammer, K. W. K.; Jain, V.; Zalis, S.; Kaim, W. *Organometallics* **2005**, *17*, 4125.
(12) Ono, K.; Joho, M. *Eur. J. Inorg. Chem.* **2006**, 3676.
(13) Prokopcova, H.; Kappe, C. O. *J. Org. Chem.* **2007**, *72*, 4440.

Table 1. Crystal Data for **1a**, **2a**, **1c**, **2c**, and **2a−OH**

compound	**1a**	**2a**	**1c**	**2c**	**2a−OH**
formula	$C_{37}H_{40}NBOSPt$	$C_{37}H_{40}NBOSPt/0.5C_6H_{14}$	$C_{40}H_{38}N_2BPt/ C_3H_6O$	$C_{40}H_{38}N_2BPt$	$C_{28}H_{30}NBO_2 SPt/2C_7H_8$
fw	752.66	795.75	810.70	752.62	834.76
crystal system	orthorhombic	monoclinic	monoclinic	orthorhombic	triclinic
space group	$P2_12_12_1$	$P2_1/c$	$P2_1/n$	*Cmca*	$P\bar{1}$
a, Å	8.8185(11)	16.465(3)	17.8308(7)	31.937(5)	11.5949(12)
b, Å	20.861(3)	9.3894(18)	8.5324(3)	11.0495(16)	13.1194(17)
c, Å	35.238(5)	24.111(5)	24.2444(9)	21.821(3)	13.8204(14)
α, deg	90	90	90	90	110.618(8)
β, deg	90	103.167(2)	105.149(2)	90	102.690(7)
γ, deg	90	90	90	90	97.594(8)
V, Å^3	6482.5(14)	3629.6(12)	3560.4(2)	7700(2)	1868.4(4)
Z	8	4	4	8	2
D_{calcd}, g cm^{-3}	1.542	1.456	1.512	1.298	1.484
T, K	180	180	180	180	180
μ, mm^{-1}	4.423	3.954	3.977	3.670	3.847
$2\theta_{max}$, deg	54.36	52.00	54.40	54.34	54.60
reflns measured	72570	33583	32681	36437	14080
reflns used	14278	7141	7881	4358	14080
parameters	774	415	441	289	421
R [$I > 2\sigma(I)$]					
R_1[a]	0.0448	0.0388	0.0566	0.0729	0.0552
wR_2[b]	0.0758	0.0845	0.0870	0.1472	0.1276
R (all data)					
R_1[a]	0.0676	0.0537	0.1525	0.2651	0.0848
wR_2[b]	0.0828	0.0911	0.1125	0.2201	0.1445
GOF on F^2	1.070	1.050	0.962	0.946	1.023

[a] $R_1 = \sum |F_o| - |F_c| / \sum |F_o|$. [b] $wR_2 = [\sum w[(F_o^2 - F_c^2)^2] / \sum [w(F_o^2)^2]]^{1/2}$, $w = 1/[\sigma^2(F_o^2) + (0.075P)^2]$, where $P = [\max(F_o^2,0) + 2F_c^2]/3$.

1H, B-*Ph*), 6.78 (s; 4H, *H*-Mes), 6.63 (m; 3H, Ph), 2.32 (s; 6H, *p*-*Me*-Mes), 2.00 (s; 12H, *o*-Me-Mes). Anal. Calcd. for $C_{40}H_{39}BN_2Pt$: C, 63.75; H, 5.22; N, 3.72. Found: C, 64.19; H, 5.01; N, 3.62.

Synthesis of Pt(*p*-ppy-B)Ph(py), 2b. To a CH_2Cl_2 (2 mL) solution of **2a** (20 mg, 0.027 mmol) was added pyridine (3 μL, 0.037 mmol). The mixture was kept standing for several hours. After the removal of solvent and washing with hexanes, the yellow powder of **2b** was obtained in 90% yield. ^{1}H NMR (500 MHz, CD_2Cl_2, 25 °C, δ, ppm): 8.68 (dd, $J = 7.5$ Hz, $J = 1.5$ Hz; 2H, py), 7.91 (dd, $J = 8.0$ Hz, $J = 1.5$ Hz; 1H, *py*-B), 7.84 (d, $J = 8.0$ Hz; 1H, *py*-B), 7.67 (d; $J = 8.0$ Hz; 1H, *Ph*-py), 7.58 (t, $J = 8.0$ Hz; 1H, py), 7.53 (s; 1H, *py*-B), 7.50 (dd, satellites, $J = 8.0$ Hz, $J = 1.0$ Hz, $J_{Pt-H} = 65.0$ Hz; 2H, Ph), 7.16 (t, $J = 8.0$ Hz; 2H, py), 7.09 (td, $J = 8.0$ Hz, $J = 1.0$ Hz; 1H, *Ph*-py), 7.05 (dd, $J = 8.0$ Hz, $J = 1.5$ Hz; 1H, *Ph*-py), 7.01 (m; 1H, *Ph*-py), 6.95 (t, $J = 7.5$ Hz; 2H, Ph), 6.86 (t, $J = 7.5$ Hz; 1H, Ph), 6.81 (s; 4H, *H*-Mes), 2.35 (s; 6, *p*-*Me*-Mes), 1.99 (s; 12H, *o*-*Me*-Mes). ^{13}C-{^{1}H}NMR (100 MHz, CD_2Cl_2, δ, ppm): 154.74, 151.07, 140.74, 139.38, 138.08, 136.88, 128.62, 127.04, 126.03, 124.64, 122.92, 121.94, 120.91, 119.00, 118.41, 23.47, 21.24. Anal. Calcd for $C_{40}H_{39}BN_2Pt \cdot$DMSO: C, 60.65; H, 5.45; N, 3.37. Found: C, 60.82; H, 5.62; N, 3.28.

Synthesis of [Pt(*p*-B-ppy)Ph]$_2$(4,4′-bipy), 1c. To an acetone solution (20 mL) of **1a** (20 mg, 0.027 mmol) was slowly added 4,4′-bipyridine (2.0 mg, 0.013 mmol) in acetone (2 mL). The mixture was kept standing at ambient temperature, and the solution was allowed to evaporate slowly. Orange crystals of **1c** were obtained after two days (90% yield). ^{1}H NMR (500 MHz, CD_2Cl_2, 25 °C, δ, ppm): 9.03 (d, $J = 5.0$ Hz; 2H, py), 7.92 (m, 2H, 5, *py*-Ph), 7.77 (d, $J = 5.0$ Hz; 1H, *py*-Ph), 7.72 (dd, $J = 5.0$ Hz, $J = 1.5$ Hz; 2H, py), 7.59 (d, $J = 8.0$ Hz; 1H, B-*Ph*), 7.29 (m, satellites; 3H, ph, B-*Ph*), 7.17 (dd, $J = 8.0$ Hz, $J = 1.0$ Hz; 1H, B-*Ph*), 7.11 (td, $J = 7.0$ Hz, $J = 1.5$ Hz; 1H, *py*-Ph), 6.80 (s, 4H, *H*-Mes), 6.70 (t, $J = 7.5$ Hz, 2H, Ph), 6.64 (t, $J = 7.5$ Hz; 1H, Ph), 2.34 (s, 6H, *p*-*Me*-Mes), 2.01 (s, 12H, *o*-*Me*-Mes). Anal. Calcd for $C_{80}H_{76}B_2N_4Pt_2$: C, 63.83; H, 5.09; N, 3.72. Found: C, 63.21; H, 5.24; N, 3.51. The acetone solvent molecules were removed by drying the sample under a vacuum.

Synthesis of [Pt(*p*-ppy-B)Ph]$_2$(4,4′-bipy), 2c. To a CH_2Cl_2 solution (10 mL) of **2a** (20 mg, 0.027 mmol) was slowly added 4,4′-bipyridine (2.0 mg, 0.013 mmol) in CH_2Cl_2 (2 mL). A total of 5 mL of hexane was layered on top. The mixture was kept standing at ambient temperature. Yellow needle crystals of **2c** were obtained overnight (85% yield). ^{1}H NMR (500 MHz, CD_2Cl_2, 25 °C, δ, ppm): 8.86 (d, $J = 6.5$ Hz; 2H, py), 7.92 (dd, $J = 8.0$ Hz, $J = 1.5$ Hz; 1H, *py*-B), 7.87 (d, $J = 8.0$ Hz; 1H, *py*-B), 7.80 (s; 1H, *py*-B), 7.70 (d, $J = 7.5$ Hz; 1H, *Ph*-py), 7.52 (d, satellites, $J = 7.0$ Hz, $J_{Pt-H} = 65.0$ Hz; 2H, Ph), 7.28 (d, $J = 6.5$ Hz; 2H, py), 7.17 (d, satellites, $J = 7.5$ Hz, $J_{Pt-H} = 42.0$ Hz; 1H, *Ph*-py), 7.05 (m; 2H, 4, 5-*Ph*-py), 6.99 (t, $J = 7.5$ Hz; 2H, Ph), 6.87 (t, $J = 7.5$ Hz; 1H, Ph), 6.69 (s, 4H, *H*-Mes), 1.98 (s, 6H, *p*-*Me*-Mes), 1.96 (s, 12H, *o*-*Me*-Mes). Anal. Calcd for $C_{80}H_{76}B_2N_4Pt_2 \cdot 1/3CH_2Cl_2$: C, 62.92; H, 5.04; N, 3.65. Found: C, 62.84; H, 5.27; N, 3.45.

X-Ray Diffraction Analysis. Single crystals of *p*-ppy-B (**2**) and complexes **1a**, **2a**, **1c**, **2c**, and **2a−OH** were mounted on glass fibers for data collection. Data were collected on a Bruker Apex II single-crystal X-ray diffractometer with graphite-monochromated Mo Kα radiation, operating at 50 kV and 30 mA and at 180 K. Data were processed on a PC with the aid of the Bruker SHELXTL software package (version 5.10)[14] and corrected for absorption effects. No significant decay was observed in all crystals except **2c**. The crystals of **2c** lose solvent rapidly when removed from solution. Attempts were made to seal the crystal along with the mother liquor in a capillary, but without success. The best data set collected for **2c** was obtained by mounting a fresh crystal quickly to a glass fiber cooled to 180 K on the goniometer head. A substantial loss of solvent molecules from the crystal lattice was still evident, which is responsible for the poor quality of the data collected for **2c** and the low diffraction intensity (only about 30% reflections have intensity greater than 2σ). None of the solvent molecules in the crystal lattice of **2c** could be located and modeled. Nonetheless, the key structural features of molecule **2c** were established. All structures were solved by direct methods. Compound **2a** contains 0.5 hexane per

(14) *SHELXTL*, version 6.14; Bruker AXS: Madison, WI, 2003.

Table 2. Selected Bond Lengths (Å) and Angles (deg) for **1a**, **2a**, **1c**, **2c**, and **2a**−**OH**

1a		**2a**−**OH**	
Pt(1A)−C(12A)	2.008(8)	Pt(1)−C(12)	2.023(6)
Pt(1A)−C(1A)	2.038(8)	Pt(1)−C(1)	2.051(6)
Pt(1A)−N(1A)	2.120(6)	Pt(1)−N(1)	2.119(5)
Pt(1A)−S(1A)	2.280(2)	Pt(1)−S(1)	2.2906(15)
Pt(1)−C(1)	2.013(7)	B(1)−O(1)	1.331(9)
Pt(1)−C(12)	2.017(7)	B(1)−C(20)	1.563(9)
Pt(1)−N(1)	2.136(6)	B(1)−C(10)	1.585(9)
Pt(1)−S(1)	2.288(2)	C(12)−Pt(1)−C(1)	92.0(2)
C(12A)−Pt(1A)−C(1A)	92.2(3)	C(12)−Pt(1)−N(1)	171.3(2)
C(12A)−Pt(1A)−N(1A)	171.6(3)	C(1)−Pt(1)−N(1)	79.7(2)
C(1A)−Pt(1A)−N(1A)	79.4(3)	C(12)−Pt(1)−S(1)	88.69(17)
C(12A)−Pt(1A)−S(1A)	89.3(2)	C(1)−Pt(1)−S(1)	177.78(16)
C(1A)−Pt(1A)−S(1A)	175.3(2)	N(1)−Pt(1)−S(1)	99.50(14)
N(1A)−Pt(1A)−S(1A)	99.02(18)	O(1)−B(1)−C(20)	124.0(5)
C(1)−Pt(1)−C(12)	90.1(3)	O(1)−B(1)−C(10)	114.8(6)
C(1)−Pt(1)−N(1)	80.3(3)	C(20)−B(1)−C(10)	121.2(6)
C(12)−Pt(1)−N(1)	170.3(3)		
C(1)−Pt(1)−S(1)	178.71(19)		
C(12)−Pt(1)−S(1)	90.1(2)		
N(1)−Pt(1)−S(1)	99.41(17)		

2a		**1c**	
Pt(1)−C(12)	2.010(5)	Pt(1)−C(1)	1.987(8)
Pt(1)−C(1)	2.021(5)	Pt(1)−C(12)	1.997(9)
Pt(1)−N(1)	2.121(4)	Pt(1)−N(2)	2.118(6)
Pt(1)−S(1)	2.2888(14)	Pt(1)−N(1)	2.124(7)
C(12)−Pt(1)−C(1)	91.7(2)	C(1)−Pt(1)−C(12)	93.5(3)
C(12)−Pt(1)−N(1)	171.22(19)	C(1)−Pt(1)−N(2)	177.7(3)
C(1)−Pt(1)−N(1)	80.34(19)	C(12)−Pt(1)−N(2)	88.8(3)
C(12)−Pt(1)−S(1)	88.79(16)	C(1)−Pt(1)−N(1)	80.3(3)
C(1)−Pt(1)−S(1)	175.47(15)	C(12)−Pt(1)−N(1)	173.5(3)
N(1)−Pt(1)−S(1)	99.48(12)	N(2)−Pt(1)−N(1)	97.4(3)

2c			
Pt(1)−C(1)	2.12(2)	N(2)−Pt(1)−C(12)	81.6(8)
Pt(1)−C(12)	1.993(18)	N(2)−Pt(1)−N(1)	96.9(7)
Pt(1)−N(1)	2.090(13)	C(12)−Pt(1)−N(1)	176.0(7)
Pt(1)−N(2)	1.990(19)	N(2)−Pt(1)−C(1)	171.2(10)
N(1)−Pt(1)−C(1)	86.8(6)	C(12)−Pt(1)−C(1)	94.2(6)

complex in the lattice, while compounds **1c** and **2a**−**OH** contain two acetone molecules and two toluene molecules per complex, respectively, which were all modeled and refined successfully. Most of the non-hydrogen atoms were refined anisotropically. The positions of hydrogen atoms were calculated, and their contributions in structural factor calculations were included. For structure **2c**, due to the sever disordering of the structure and the lack of sufficient data, most of the carbon atoms were refined isotropically. The crystal data of the complexes are given in Table 1. Important bond lengths and angles for all of the compounds are listed in Table 2. Data for *p*-ppy-B are provided in the Supporting Information.

Results and Discussion

Syntheses. As shown in Scheme 1, the synthesis of *p*-B-ppy (**1**) was achieved by Suzuki-Miyaura coupling of 4-bromophenylboronic acid with 2-bromopyridine, followed by substitution of the bromo group with $BMes_2$ in THF. This is a different procedure from the previously reported one for compound **1** where Stille coupling methods were used.[5d] Compound **2**, *p*-ppy-B, was achieved by Suzuki coupling of phenylboronic acid and 2,5-dibromopyridine, followed by substitution of the bromo group with $BMes_2$ in diethyl ether. The DMSO complexes Pt(*p*-B-ppy)Ph(DMSO) (**1a**) and Pt(*p*-ppy-B)Ph(DMSO) (**2a**) were obtained readily by cyclometalation reactions of $PtPh_2(DMSO)_2$ with ligands **1** and **2**, respectively, in THF at 50 °C. Because DMSO in **1a** and **2a** is a relatively weak donor, it can be replaced readily by other donor ligands such as pyridine, leading to the pyridine complexes Pt(*p*-B-ppy)Ph(py) (**1b**) and Pt(*p*-ppy-B)Ph(py) (**2b**), respectively. Similarly, metal complexes $[Pt(p\text{-B-ppy})]_2(4,4'\text{-bipy})$ (**1c**) and $[Pt(p\text{-ppy-B})]_2(4,4'\text{-bipy})$ (**2c**) were obtained by reacting 0.5 equiv of 4,4′-bipy with 1 equiv of **1a** and **2a**, respectively. The free ligands and all Pt(II) complexes were fully characterized by NMR, high-resolution mass spectrometry (HRMS), or elemental analyses, and the structures of the metal complexes are illustrated in Chart 2.

Structures. The crystal structure of *p*-ppy-B was determined by single-crystal X-ray diffraction analysis and is shown in Figure 1. The phenyl and the pyridyl planes are off coplanarity by 23.6°. The structures of complexes **1a**, **2a**, **1c**, and **2c** were also established by single-crystal X-ray diffraction analyses and are shown in Figures 2−5, respectively.

1a, 2a, and 2a−**OH.** The crystal structures shown in Figure 2 established unequivocally that the auxiliary ligand DMSO in **1a** and **2a** is bound to the Pt(II) center trans to the phenyl ring, not the pyridyl ring, of the ppy

Scheme 1

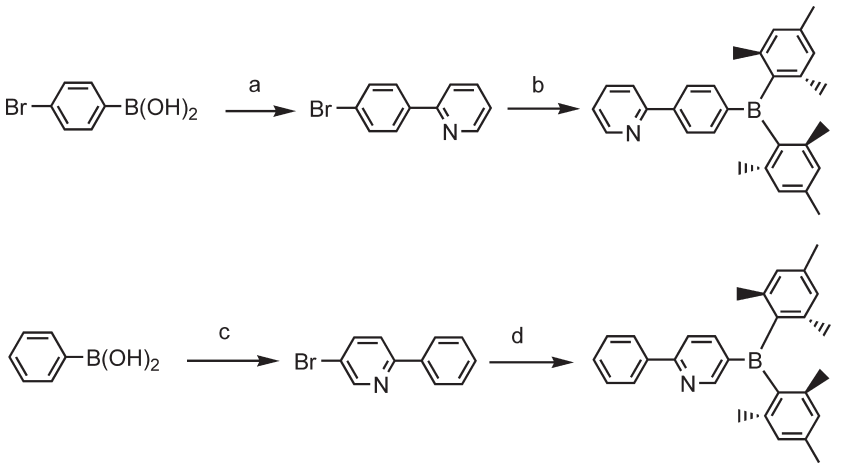

Reagents and conditions: a) 2-bromopyridine, $Pd(PPh_3)_4$, and NaOH, toluene, alcohol, and water (3:1:1), rt. 48 h; b) (i) n-BuLi, THF, −78 °C; (ii) $B(Mes)_2F$, −78 °C to rt, overnight; c) 2, 5-bromopyridine, $Pd(PPh_3)_4$, and NaOH, toluene, alcohol, and water (3:1:1), rt. 48 h; d) (i) n-BuLi, Et_2O, −78 °C; (ii) $B(Mes)_2F$, −78 °C to rt, overnight.

Chart 2

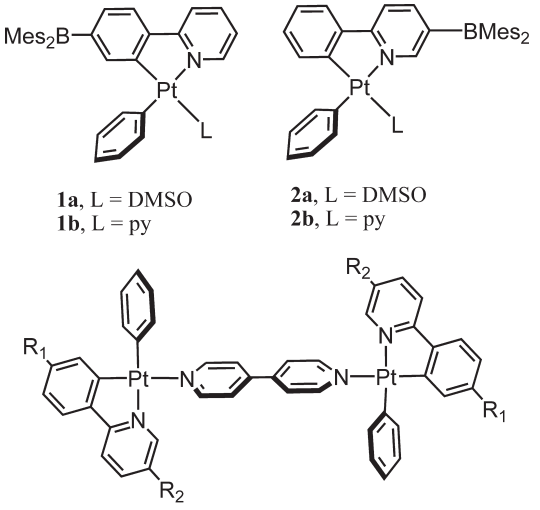

1a, L = DMSO
1b, L = py

2a, L = DMSO
2b, L = py

1c, R_1=$BMes_2$; R_2= H
2c, R_1=H; R_2=$BMes_2$

chelate. NMR spectra confirmed that this cis isomer (the two phenyl rings being cis to each other) is formed exclusively for both **1a** and **2a**. This can be explained by the well-established intramolecular C−H bond activation mechanism on a Pt(II) center[11] depicted for the formation of complex **1a** in Scheme 2. The greater trans effect exerted by the phenyl ring of ppy in the five-coordinate Pt(IV) intermediate leads to the regioselective reductive elimination of the phenyl group trans to it along with the H atom from the Pt(IV) center as a benzene molecule. The subsequent DMSO coordination gives rise to complex **1a**. Similar regioselective cyclometalation reactions involving a Pt(II) center have been observed previously.[5h,15,16]

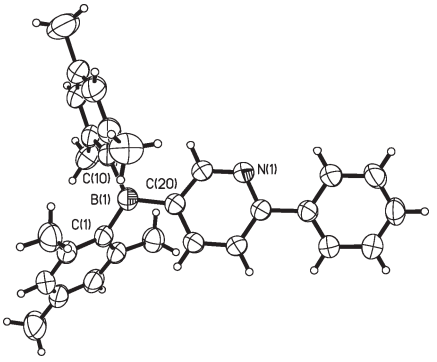

Figure 1. The structure of *p*-ppy-B with 50% thermal ellipsoids.

In the asymmetric unit of **1a**, there are two independent molecules that form a stacked pair with a Pt−Pt separation distance of 4.906(1) Å (see Supporting Information). The Pt−C, Pt−N, and Pt−S bond lengths and angles in **1a** and **2a** are similar. One common feature in the structures of **1a** and **2a** is that the oxygen atom of the DMSO ligand is oriented toward the *ortho*-H atom of the pyridyl ring with the $C_o\cdots O$ and $H_o\cdots O$ separation distances being 2.98−3.04 Å and 2.13−2.19 Å, respectively. The key difference between these two structures is that in **1a** the DMSO ligand is far away from the $BMes_2$ group, while in **2a** it is close to the $BMes_2$ group. In fact, the separation distance between O(1) and B(1) in **2a** is only 4.58(2) Å, and that between O(1) and C(29) is 4.07 Å.

There is also a notable difference in the stabilities of **1a** and **2a** toward adventitious H_2O molecules in solution. Compound **1a** is stable in solution under air for a long period of time, while **2a** undergoes slow decomposition under air with nearly quantitative formation of a new compound Pt[*p*-ppy-BMes(OH)]Ph(DMSO) (**2a**−**OH**), which was fully characterized by NMR, elemental analysis, and single-crystal X-ray diffraction. The structure of **2a**−**OH** is shown in Figure 3.

The Pt−ligand bond lengths and angles of **2a**−**OH** are similar to those of **1a** and **2a**. The B−O bond length of

(15) Zhao, S. B.; Wang, R. Y.; Wang, S. *J. Am. Chem. Soc.* **2007**, *129*, 3092.
(16) Yagyu, T.; Ohashi, J. I.; Maeda, M. *Organometallics* **2007**, *26*, 2383.

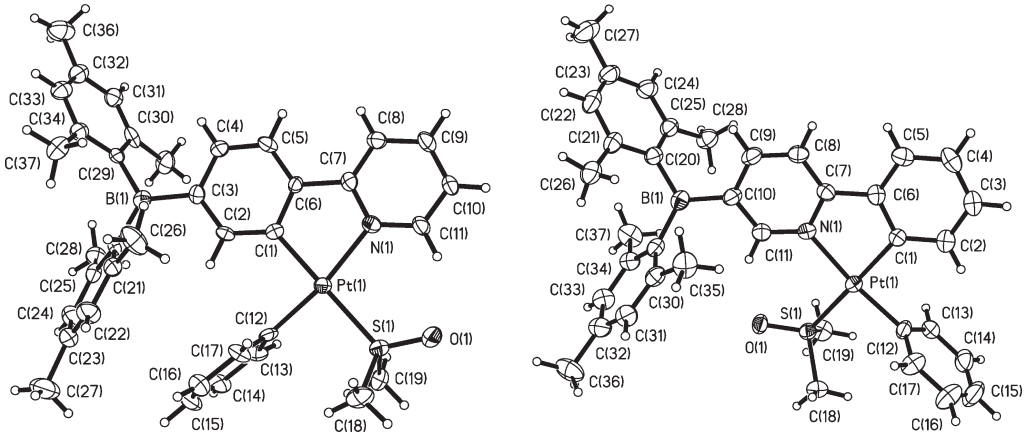

Figure 2. The structures of **1a** (left) and **2a** (right) with 50% thermal ellipsoids and labeling schemes.

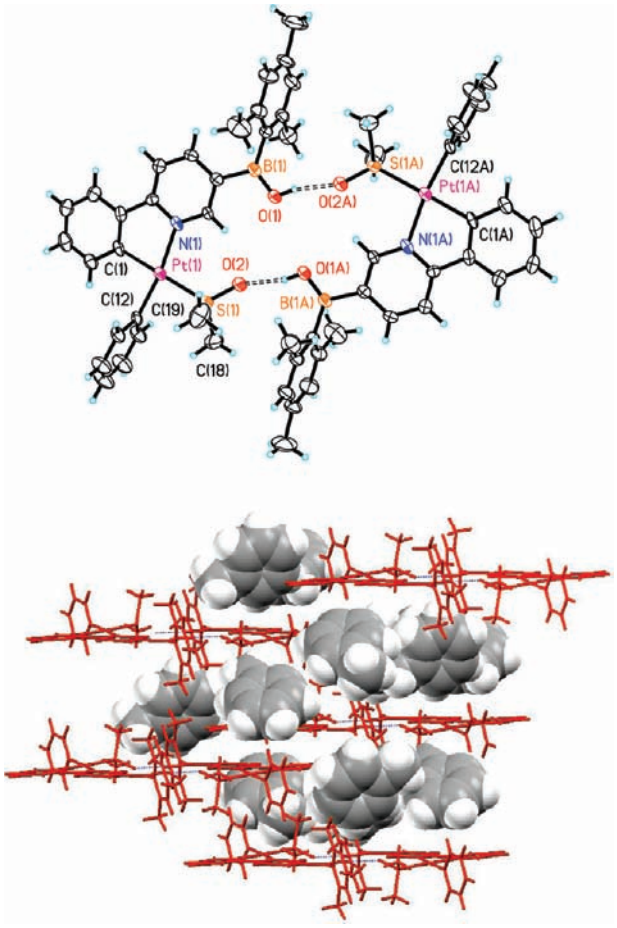

Figure 3. Top: The hydrogen bonded dimer of **2a**−**OH**. Bottom: Crystal lattice packing diagram showing the toluene solvent molecules in the lattice.

1.331(9) Å is much shorter than that of a typical B−O single bond (∼1.50−1.55 Å, e.g., Ph_2Bq, q = 8-hydroxyquinoline anion and derivatives),[17] clearly supporting a B=O double bond. When the water-free solution of **2a** is kept under nitrogen, **2a** does not show any sign of decomposition. Hence, we attributed the decomposition of **2a** to an internal DMSO-facilitated B−C bond hydrolysis process, as illustrated in Scheme 3. The greater Lewis acidity and the close proximity to the DMSO ligand of the $BMes_2$ group in **2a**, compared to that in **1a**, are believed to be responsible for the unusual decomposition of the ppy-B ligand.

Interestingly, as shown in Figure 3, the molecule of **2a**−**OH** forms a hydrogen-bond-linked dimer through the DMSO oxygen atom and the hydroxo group in the crystal lattice. Each of these dimers stacks with a neighboring dimer with a Pt−Pt separation distance of 5.189(1) Å (see Supporting Information). Furthermore, compound **2a**−**OH** forms a highly porous crystal lattice that hosts two toluene solvent molecules per complex (Figure 3).

1c and 2c. As shown in Figures 4 and 5, complexes **1c** and **2c** display a similar cis structure to those of **1a** and **2a**, with the two pyridyl rings being cis to each other on the same Pt(II) center. Hence, the replacement of the DMSO ligand by 4,4′-bipy does not alter the cis structure of the complexes due to the strong trans effect of the phenyl group. The N(1)−Pt(1)−C((12) (173.5(3)°) and N(2)−Pt(1)−C(1) (177.7(3)°) angles in **1c** are much less distorted from linearity, compared to the corresponding S−Pt−C bond angles in **1a** and **2a**. This may be attributed to the greater steric interactions imposed by DMSO in **1a** and **2a**. The intramolecular Pt−Pt separation distance in **1c** is 11.375(1) Å, much longer than the shortest intermolecular Pt−Pt distance, 8.532(1) Å. The molecule of **1c** has a crystallographically imposed inversion center. The two $BMes_2$ groups have an anti configuration with a 22.1 Å separation distance between the two B atoms. In solution, the syn configuration is also possible due to the free rotation around the Pt−N (bipy) bond or the C(20)−C(20′) bond, which was in fact confirmed by variable-temperature ^{1}H NMR that shows the presence of two isomers at ∼185 K (see Supporting Information).

The molecule of **2c** has a crystallographically imposed inversion center and a mirror plane symmetry on which the two Pt atoms and the entire bipy linker lie. As a consequence of the mirror plane symmetry, the entire molecule of **2c** is disordered over the two sites related by mirror plane reflection. Although we have been able to model the disorder successfully, the quality of the structure data is poor due to both disordering and the poor

(17) Cui, Y.; Liu, Q. D.; Bai, D. R.; Jia, W. L.; Tao, Y.; Wang, S. *Inorg. Chem.* **2005**, *44*, 601.

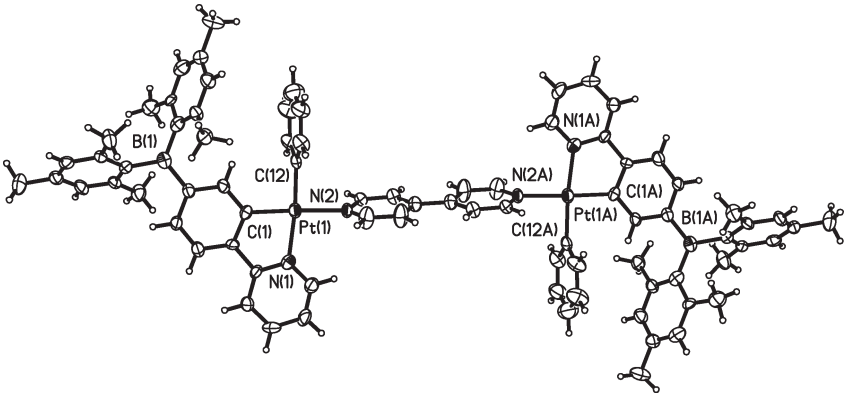

Figure 4. The structure of **1c** with 50% thermal ellipsoids and labeling schemes.

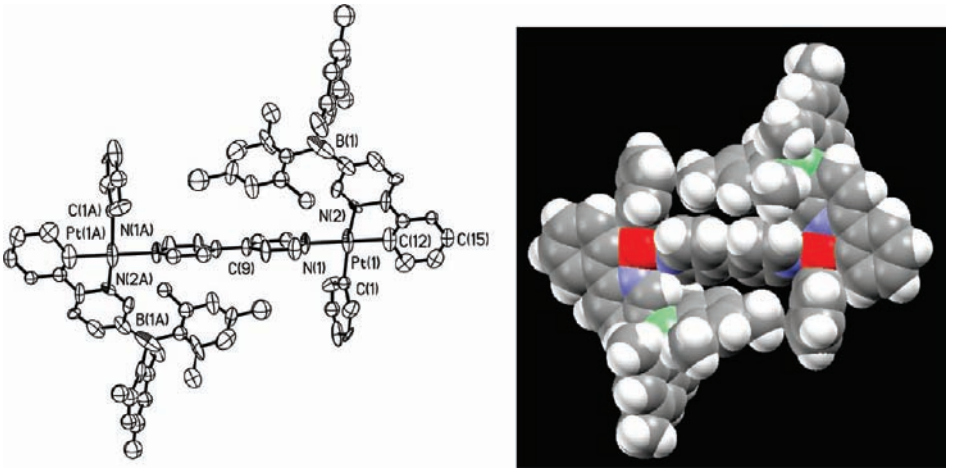

Figure 5. Left: The structure of **2c** with 50% thermal ellipsoids and labeling schemes. Hydrogen atoms are omitted. Right: A space-filling diagram showing the steric congestion in **2c**.

Scheme 2

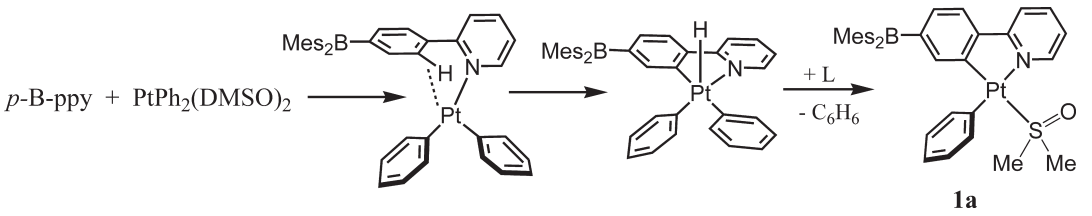

Scheme 3

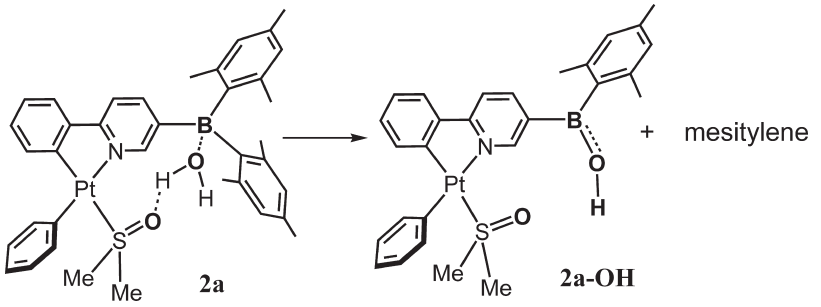

quality of the diffraction data (see Experimental Section). Because of the disordering, the structure of **2c** in the solid state could have either a syn or an anti configuration with respect to the relative orientation of the two $BMes_2$ groups, with the anti configuration of the two $BMes_2$ groups being the less congested and, thus, the more favored one. The separation distance of the two B atoms in the anti configuration shown in Figure 5 is 13.2 Å, much

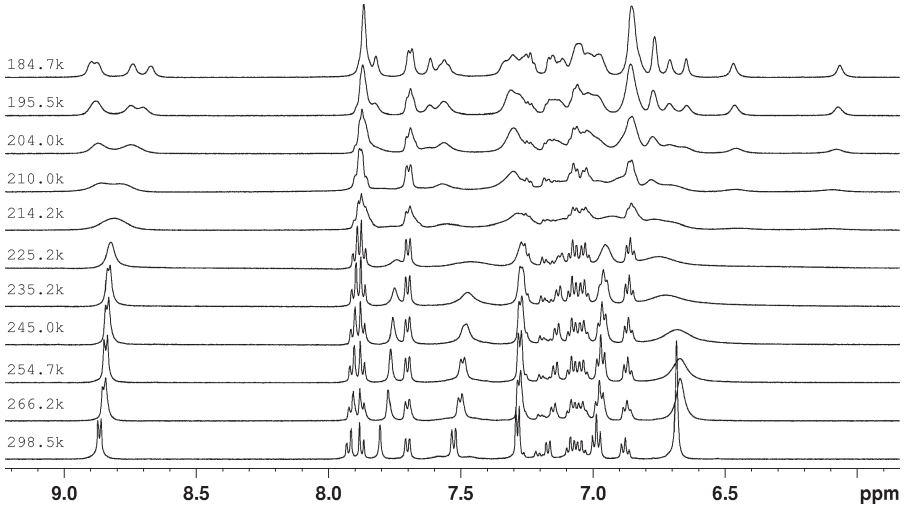

Figure 6. Variable-temperature ^{1}H NMR spectra of the aromatic region of **2c** in CD_2Cl_2.

Chart 3

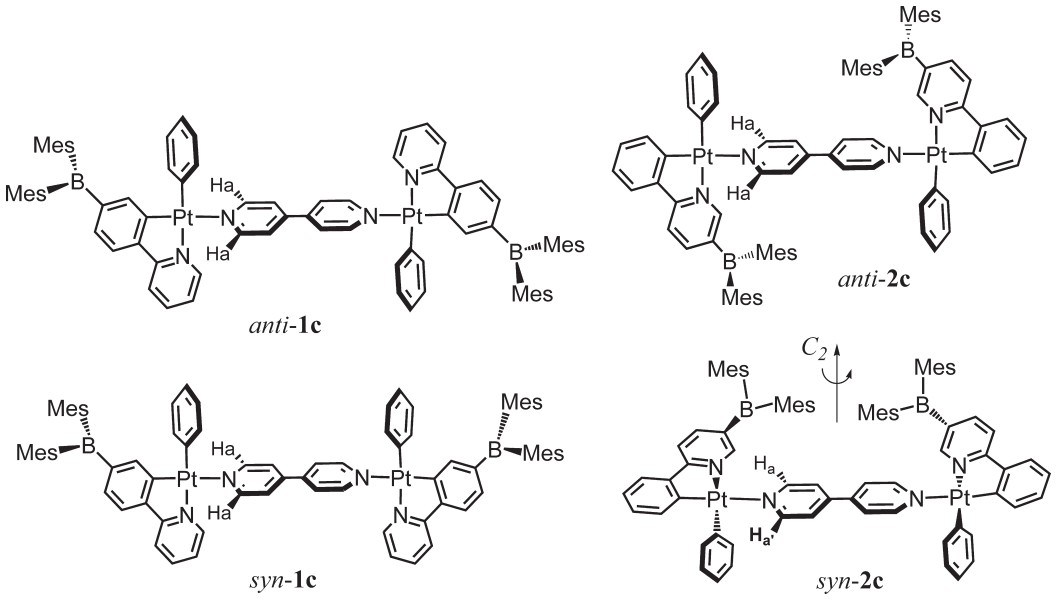

shorter than that of **1c**. Although the structures of **1b** and **2b** were not determined due to the lack of suitable crystals, the coordination environments around the Pt center are believed to be similar to those of **1c** and **2c** molecules.

To establish the structure of **2c** in solution, we recorded its variable-temperature ^{1}H NMR spectra. As shown in Figure 6, at ~200 K in CD_2Cl_2, two sets of well-resolved ortho-Ha peaks from the 4,4′-bipy ligand were observed in the 8.6−9.0 ppm region, which can be attributed to the syn and anti isomers. Lowering the temperature further to 185 K causes the splitting of each peak into two, which can be attributed to the H_a and $H_{a'}$ protons shown in Chart 3. This can be explained by the C_2 symmetry of both isomers and the apparent lack of a mirror plane symmetry, due to the strong steric interactions. The activation barrier for the anti and syn configuration interconversion of **2c** was estimated to be 41 kJ mol^{-1} on the basis of the variable-temperature NMR data. For **1c**, the syn and anti chemical shifts of the H_a protons are still very broad and not fully resolved at 185 K, and the activation energy was estimated to be 38 kJ mol^{-1}. The relatively smaller barrier of **1c** compared to that of **2c** is consistent with the more relaxed structure of **1c**. Hence, we have established that the two constitutional isomers of B-ppy and ppy-B do have a distinct impact on the structure of the Pt(II) complexes in solution and the solid state.

Absorption Spectra. The absorption spectra of the free liand *p*-B-ppy and *p*-ppy-B are shown in Figure 7 along with those of the Pt(II) complexes. The π to π^* absorption band of ppy-B (**2**) is slightly red-shifted (333 nm) compared to that of B-ppy (**1**; 329 nm). The Pt(II) complexes of *p*-B-ppy and *p*-ppy-B display absorption bands similar to those of the corresponding free ligand and a new well-resolved MLCT band with moderate intensity in the 380−500 nm region. Compared to the free ligand, the π to π^* absorption band is red-shifted, due to the enhanced π conjugation via metal chelation. For Pt(II) complexes, with the same auxiliary ligand, the MLCT absorption band of the *p*-ppy-B complexes is

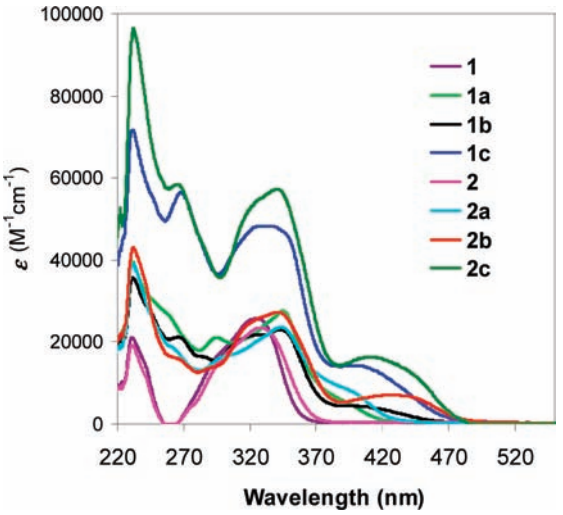

Figure 7. UV−vis absorption spectra of free ligands and the Pt(II) complexes recorded in CH_2Cl_2.

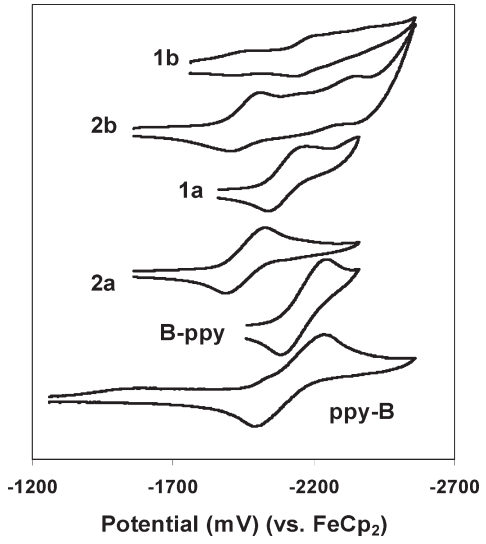

Figure 8. The CV diagrams for the free ligands and Pt(II) complexes recorded in DMF.

red-shifted relative to that of *p*-B-ppy complexes, which is in agreement with the fact that the pyridyl ring in conjugation with the boron center is more effective in lowering the π^* energy level than the phenyl ring. The extinction coefficients of the dinuclear complexes **1c** and **2c** are nearly twice those of the corresponding mononuclear compounds **1b** and **2b**. For both *p*-B-ppy and *p*-ppy-B series, the MLCT energy follows the order of DMSO > 4,4′-bipy ≈py, supporting the position that the electron-donating ability of the ligands to the Pt(II) center follows the order DMSO < 4,4′-bipy ≈py.

Electrochemical Properties. The reduction potentials of the free ligands and the Pt(II) metal complexes were recorded by cyclic voltammetry (CV; DMF as the solvent, NBu_4PF_6 as the electrolyte). As shown in Figure 8 and Table 3, the reduction potential of *p*-ppy-B (**2**) (−2.12 V, vs $FeCp_2^{0/+}$) is a little more positive than that of *p*-B-ppy (**1**), −2.16 V, supporting the position that the pyridine ring can enhance the electron-accepting ability of the boron center more effectively than the phenyl ring, consistent with our earlier reports.[5b,c] Both *p*-ppy-B Pt(II) complexes **2a** and **2b** display a reduction potential of −1.96 V, which is more positive than that of **2**. However, for the *p*-B-ppy Pt(II) complexes **1a** and **1b**, the impact of Pt(II) chelation to the *p*-B-ppy ligand is either very small or negligible, as shown by the potentials of complexes **1a** and **1b** (**1b** has very poor solubility in DMF, which resulted in the weak CV peak; −2.10 and −2.17 V, respectively), indicating that metal binding to the N, C-chelate is somewhat more effective in enhancing the electron-accepting ability of the molecule when the $BMes_2$ group is on the py ring. This is also consistent with our earlier finding on the Pt(II)-chelation-enhanced electron-accepting ability of 7-azaindolyl-derivative N,C-chelate ligands with $BMes_2$ on the N-heterocyclic ring.[5g]

Table 3. Electrochemical Data[a]

compound	*p*-B-ppy	**1a**	**1b**	*p*-ppy-B	**2a**	**2b**
$E_{1/2}^{red1}$ (V)	−2.16	−2.10	−2.17	−2.12	−1.96	−1.96

[a] All potentials are relative to $FeCp_2^{0/+}$, measured in DMF, using NBu_4PF_6 as the electrolyte with scan rates of 100−1000 mV. [complex] = ~0.003 M or less, $[NBu_4(PF_6)]$ = 0.10 M.

For complex **2b**, a second reduction peak at −2.34 V is also observed, which can be ascribed to the py ring reduction.[9a] CV data of the dinuclear Pt(II) complexes **1c** and **2c** could not be obtained due to their poor solubility in DMF.

Luminescence. Under UV irradiation, *p*-B-ppy and *p*-ppy-B both display blue luminescence in solution (CH_2Cl_2) at ambient temperature, with λ_{max} = 409 nm (Φ = 0.16) for *p*-B-ppy and 412 nm (Φ = 0.01) for *p*-ppy-B. As shown in Figure 9, the emission of *p*-B-ppy has a much stronger dependence (e.g., λ_{em} = 376 nm in hexane, 425 nm in DMF) on the solvent polarity than that of *p*-ppy-B (λ_{em}=409 nm in hexane, 428 nm in DMF), indicating a more polarized excited state than that of *p*-B-ppy.

In contrast to the free ligands, the emissions of the Pt(II) complexes are all dominated by phosphorescence. The luminescent data of the complexes are summarized in Table 4. The ambient temperature emission spectra of the complexes are shown in Figure 10. For a given ancillary ligand, the emission maximum of the *p*-B-ppy complexes is in general red-shifted by a few nanometers, compared to the *p*-ppy-B complexes. This trend is opposite that of the MLCT absorption band in the UV−vis spectra. For **1a** and **2a**, well-resolved vibronic fine features are observed in the emission spectra at ambient temperature, indicative of ligand-centered emission. The emission red shift of the *p*-B-ppy complexes relative to those of *p*-ppy-B can be therefore attributed to the greater polarized excited state of the former, as revealed by the free ligands. For **1b**, **2b**, **1c**, and **2c**, the ambient temperature emission spectra are broader than those of **1a** and **2a** and the vibronic fine features are less obvious. However, at 77 K (Figure 11), the emission spectra of all Pt(II) complexes display well-defined vibrational features, supporting the position that ligand-centered emission dominates in these complexes. The fact that the emission maxima of the Pt(II) complexes show little change with temperature also supports the position that the emission is dominated by a ^{3}LC excited state since MLCT-dominated emission is known to have a greater dependence on temperature.[13] There is a notable shoulder

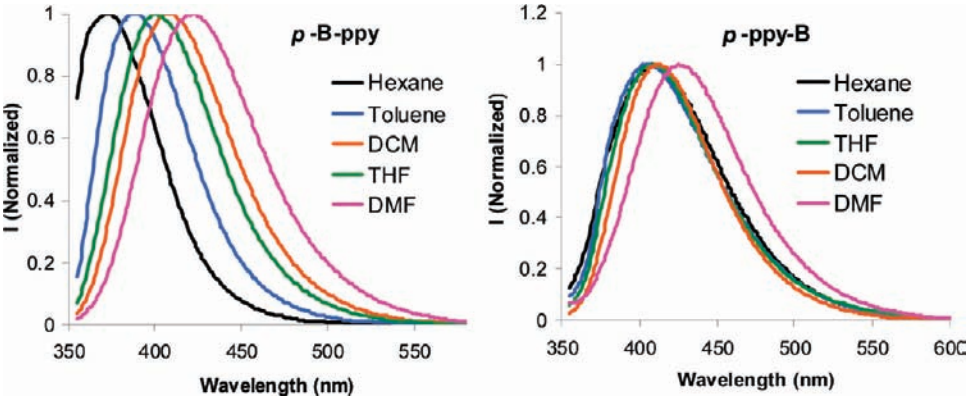

Figure 9. The emission spectra of *p*-B-ppy and *p*-ppy-B in various solvents with $\lambda_{ex} = 345$ nm, concentration = $\sim 1.0 \times 10^{-5}$ M.

Table 4. Absorption and Luminescence Data

compound	abs, nm (ε, M^{-1} cm^{-1})	λ_{em}, nm /τ, μs[a] (CH_2Cl_2, rt)	λ_{em}, nm /τ, μs (CH_2Cl_2, 77 K)	Φ[b] (CH_2Cl_2, rt)
1, *p*-B-ppy	326 (25 750)	409		0.16
2, *p*-ppy-B	329 (23 450)	412		0.012
1a	344 (27 550)	515/14.7(1)	511/28.2(1)	0.004
	392 (5400)			
2a	345 (24 500)	509/24.1(1)	501/40.2(1)	0.01
	394 (8300)			
1b	343 (22 950)	543/7.1(1)	538/13.4(2)	0.03
	411 (4050)			
2b	345 (26 850)	534/8.1(1)	525/14.0(1)	0.03
	425 (7050)			
1c	343 (47 300)	543/8.8(2)	541/13.1(1)	0.006
	411 (13 300)			
2c	344 (56 600)	535/7.1(1)	530/12.5(1)	0.003
	425 (15 400)			

[a] The decay lifetime at rt for the Pt(II) complexes was measured under N_2. [b] The quantum efficiency for the free ligands was obtained under air using 9,10-diphenylanthracene as the standard. For the Pt(II) complexes, the quantum efficiency was measured under N_2 using $Ir(ppy)_3$ as the standard ($\Phi = 0.40$).[9a]

peak in the emission spectrum of **1b** at ~485 nm at 298 K, which is resolved with fine vibronic features at 77 K. This peak is insensitive to oxygen and, thus, attributed to ligand-based singlet emission.

For either *p*-B-ppy or *p*-ppy-B complexes, the emission maxima of the 4,4′-bipy and py complexes are similar but about 30 nm red-shifted, compared to those of the corresponding DMSO complexes. This trend is consistent with that of the MLCT band observed in the UV−vis absorption spectra. Hence, some MLCT contributions to the phosphorescent emission band are very likely. Compared to Pt(ppy)(acac) and its derivatives,[9a] the quantum efficiencies of complexes **1a**, **1b**, **2a**, and **2b** are either much lower or comparable. Although the diplatinum complexes **1c** and **2c** have similar absorption and emission spectra to those of the corresponding monoplatinum complexes **1b** and **2b**, their emission quantum efficiency is however much lower than that of the mononuclear complexes, which may be attributed to intramolecular triplet−triplet quenching.

Molecular Orbital Calculations. To understand the origin of the electronic transitions in the free ligands and the metal complexes, DFT calculations for *p*-B-ppy and *p*-ppy-B and their Pt(II) complexes **1b** and **2b** were performed using the Gaussian 03 package with the B3LYP/6-311++G** basis set.[18,19] The geometrical parameters obtained for *p*-ppy-B, **1c**, and **2c** from X-ray diffraction experiments were used as the starting point for the geometry optimization of *p*-ppy-B, **1b**, and **2b**.

The highest occupied molecular orbital (HOMO) and lowest unoccupied molecular orbital (LUMO) diagrams of *p*-B-ppy (**1**) and *p*-ppy-B (**2**) are shown in Figure 12. The HOMO of **1** consists of contributions nearly exclusively from the mesityls, while the LUMO is dominated by the p_π orbital of the boron atom with significant contributions from the pyridyl and phenyl ring. The LUMO level of **2** closely resembles that of **1**, but the HOMO level has significant contributions from the pyr-

(18) Frisch, M. J.; Trucks, G. W.; Schlegel, H. B.; Scuseria, G. E.; Robb, M. A.; Cheeseman, J. R.; Montgomery, J. A., Jr.; Vreven, T.; Kudin, K. N.; Burant, J. C.; Millam, J. M.; Iyengar, S. S.; Tomasi, J.; Barone, V.; Mennucci, B.; Cossi, M.; Scalmani, G.; Rega, N.; Petersson, G. A.; Nakatsuji, H.; Hada, M.; Ehara, M.; Toyota, K.; Fukuda, R.; Hasegawa, J.; Ishida, M.; Nakajima, T.; Honda, Y.; Kitao, O.; Nakai, H.; Klene, M.; Li, X.; Knox, J. E.; Hratchian, H. P.; Cross, J. B.; Adamo, C.; Jaramillo, J.; Gomperts, R.; Stratmann, R. E.; Yazyev, O.; Austin, A. J.; Cammi, R.; Pomelli, C.; Ochterski, J. W.; Ayala, P. Y.; Morokuma, K.; Voth, G. A.; Salvador, P.; Dannenberg, J. J.; Zakrzewski, V. G.; Dapprich, S.; Daniels, A. D.; Strain, M. C.; Farkas, O.; Malick, D. K.; Rabuck, A. D.; Raghavachari, K.; Foresman, J. B.; Ortiz, J. V.; Cui, Q.; Baboul, A. G.; Clifford, S.; Cioslowski, J.; Stefanov, B. B.; Liu, G.; Liashenko, A.; Piskorz, P.; Komaromi, I.; Martin, R. L.; Fox, D. J.; Keith, T.; Al-Laham, M. A.; Peng, C. Y.; Nanayakkara, A.; Challacombe, M.; Gill, P. M. W.; Johnson, B.; Chen, W.; Wong, M. W.; Gonzalez, C.; Pople, J. A. *Gaussian 03*, revision C.2; Gaussian, Inc.: Wallingford, CT, 2004.

(19) (a) Becke, A. D. *J. Chem. Phys.* **1993**, *98*, 5648. (b) Lee, C.; Yang, W.; Parr, R. G. *Phys. Rev. B* **1988**, *37*, 785. (c) Miehlich, B.; Savin, A.; Stoll, H.; Preuss, H. *Chem. Phys. Lett.* **1989**, *157*, 200. (d) Hariharan, P. C.; Pople, J. A. *Theor. Chim. Acta* **1973**, *28*, 213.

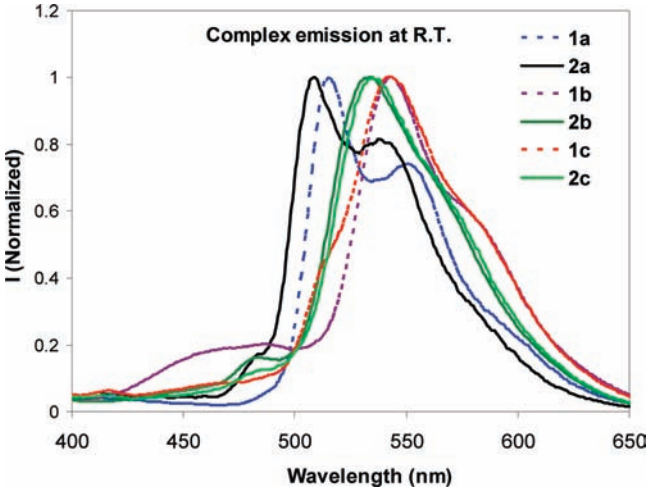

Figure 10. Emission spectra of complexes in CH_2Cl_2, ~1.0×10^{-5} M, under N_2 at 298 K.

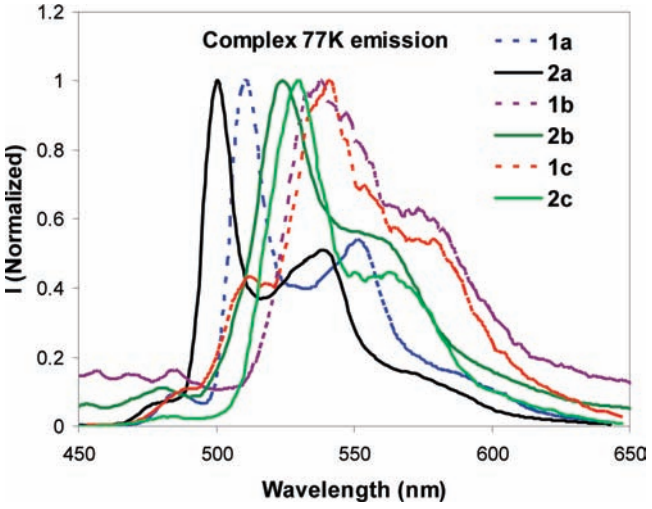

Figure 11. Emission spectra of complexes in CH_2Cl_2, ~1.0×10^{-5} M, under N_2 at 77 K.

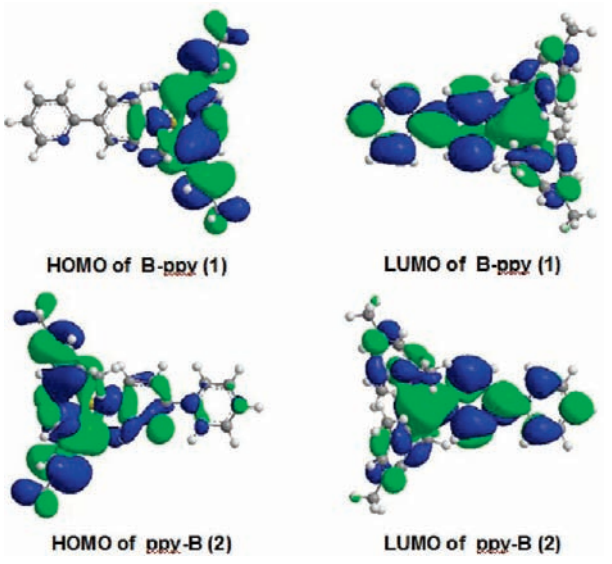

Figure 12. HOMO and LUMO orbitals of free ligands B-ppy and ppy-B, plotted with a 0.015 isocontour value.

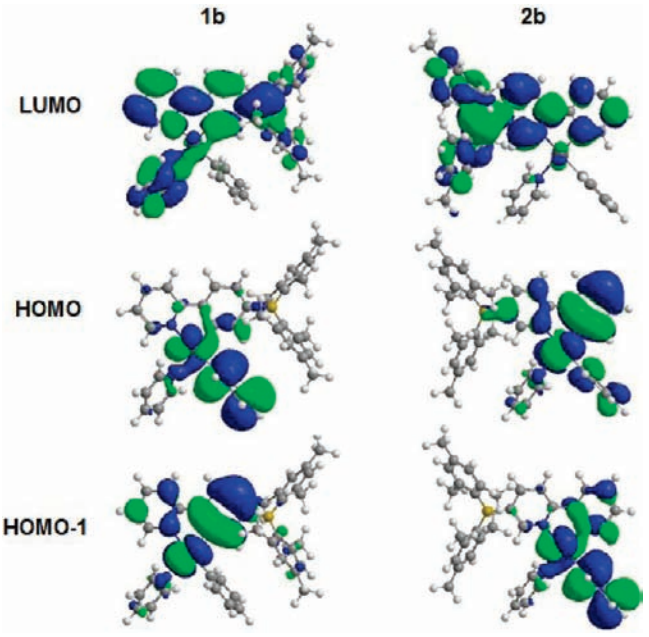

Figure 13. HOMO and LUMO orbitals of **1b** and **2b**, plotted with a 0.015 isocontour value.

idyl ring, in addition to the mesityls. Hence, although the lowest electronic transition for both **1** and **2** may be described as charge transfer from mesityl to the B-ppy or ppy-B unit, for **2**, due to the direct conjugation of the pyridyl ring with the B atom, its excited state is less polarized than that of **1**, thus explaining the greater solvent-dependent emission of **1**.

As shown in Figure 13, the HOMO of **1b** is dominated by the π orbitals of the phenyl group with some contributions from the Pt d orbitals. However, HOMO−1, which is very close in energy to HOMO (0.001 hartree difference), is a π orbital centered on the phenyl portion of the ppy chelate with significant d orbital contributions of the Pt(II) ion. The LUMO of **1b** is a π^* orbital dominated by the B atom and the ppy chelate with significant contributions from the py ligand. For **2b**, HOMO and HOMO−1 are nearly identical in energy (0.0007 hartree difference), with HOMO being the π orbital localized on the ppy ring and the Pt atom and HOMO−1 being the phenyl π orbital with some Pt d orbital contributions. The LUMO of **2b** is a π^* orbital similar to that of **1b** but with no significant contributions from the py ligand. Hence, the lowest electronic transitions in **1b** and **2b** likely involve both $\pi \rightarrow \pi^*$ transitions localized on the B-ppy chelate and interligand charge transfer from phenyl to the B-ppy ligand, with MLCT contributions in both transitions, in agreement with UV−vis and luminescent data.

Lewis Acidity—Response to Fluoride Ions. Since triarylboron groups such as $B(Ar)Mes_2$ are well-known to bind to fluoride ions with a high selectivity,[3,4] we examined the Lewis acidity of the boron center in the Pt(II) complexes by carrying out the fluoride titration experiments in both absorption and luminescence modes.

***p*-B-ppy and *p*-ppy-B.** As shown in Figure 14, upon the addition of TBAF in CH_2Cl_2, the low-energy absorption bands at 327 and 330 nm, respectively, in the spectra of *p*-B-ppy (**1**) and *p*-ppy-B (**2**) are quenched and blue-

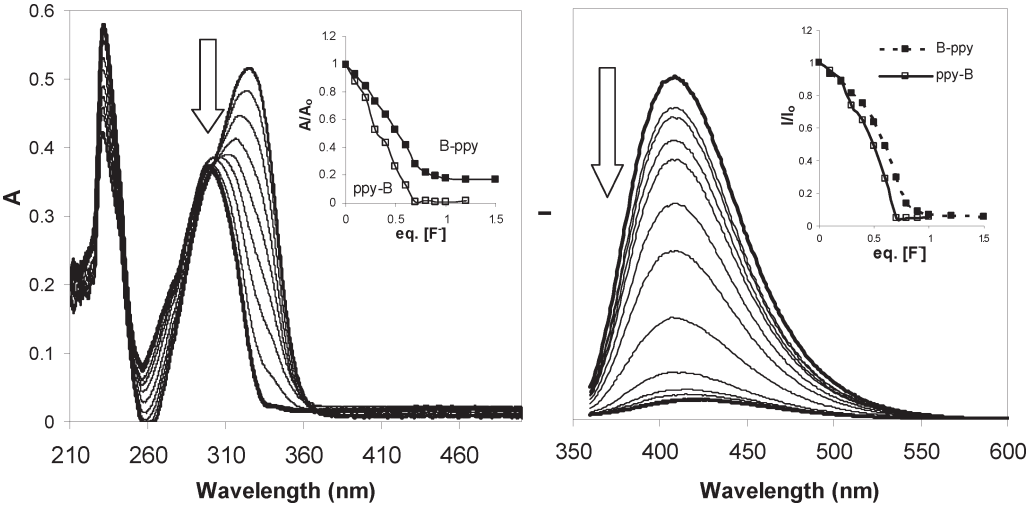

Figure 14. UV−vis (left) and fluorescent (right) spectral change of **1** (2.0×10^{-5} M) with the addition of NBu_4F in CH_2Cl_2. Inset: Plots of A/A_o or I/I_o vs equiv of [F^-] at λ_{max} for both **1** and **2**. The UV−vis and fluorescent titration spectra of **2** are provided in the Supporting Information.

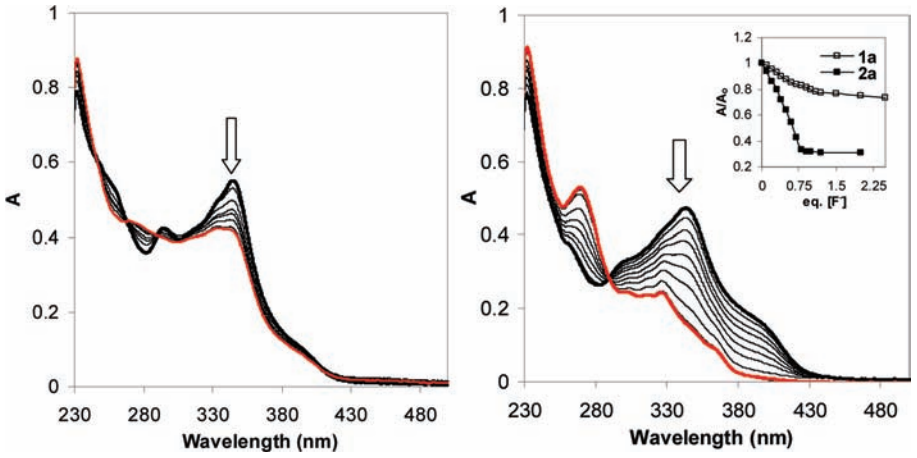

Figure 15. The UV−vis spectral change of **1a** (left) and **2a** (right) (2.0×10^{-5} M) with the addition of NBu_4F in CH_2Cl_2. Inset: A/A_0 vs equiv [F^-] plots at 345 nm for both **1a** and **2a**.

shifted. The saturation point is reached for both compounds with ~1.0 equiv of F^- added, an indication that both molecules bind to fluoride fairly strongly. Nonetheless, the plots of A/A_o versus the equivalents of F^- added show clearly that the *p*-ppy-B has a somewhat stronger binding toward F^- than *p*-B-ppy, which is consistent with its greater electron-accepting ability, as established by the CV data, thus demonstrating that the direct conjugation of a pyridyl ring with the $BMes_2$ group is more efficient in enhancing the Lewis acidity of the boron center than the phenyl group. In the fluorescent spectra, the emission band of both compounds undergoes similar quenching with the addition of fluoride. Again, the ppy-B molecule shows a slightly stronger binding with fluoride than B-ppy does.

Pt(II) Complexes. Absorption Titration. Unlike the free ligands, the response of the Pt(II) complexes **1a** and **2a** toward fluorides is quite different. As shown by the UV−vis spectra in Figure 15, the addition of excess TBAF (~4 equiv) to the solution of **1a** causes only a 20% decrease of the intense π to π^* peak at 347 nm and very little change of the MLCT band between 380 and 450 nm. In contrast, both π to π^* and MLCT bands in **2a** experience about an 80% decrease of intensity and reach a saturation point with ~1 equiv of F^-, indicating its strong binding with fluorides. The same trend was also observed between **1b** and **2b** and between **1c** and **2c**, as shown by the titration spectra and the A/A_o versus equivalent [F^-] plots in Figures 16 and 17.

The binding constants of **1a** and **1b** with fluoride ions were found to be 9×10^5 M^{-1} and 1×10^5 M^{-1}, respectively, which are about 100 times smaller than those of **2a** and **2b** (~10^7 M^{-1} to 10^8 M^{-1}; see Supporting Information). The weaker response of the *p*-B-ppy Pt(II) complexes toward fluoride can be attributed to the weaker electron-accepting ability of the boron center in the *p*-B-ppy complexes, relative to that of the *p*-ppy-B complexes, as supported by the CV data. Compared to the free *p*-B-ppy ligand ($K = \sim 6 \times 10^7$ M^{-1}), the response of **1a**, **1b**, and **1c** toward fluoride is much weaker, which can be explained by steric factors. If both the ligand and the complex show similar reduction potentials, the Lewis acidity of the metal complexes would be lower than that of the free ligand due to the greater steric interaction imposed by the binding of fluoride in the complex, which is the case for the *p*-B-ppy complexes.

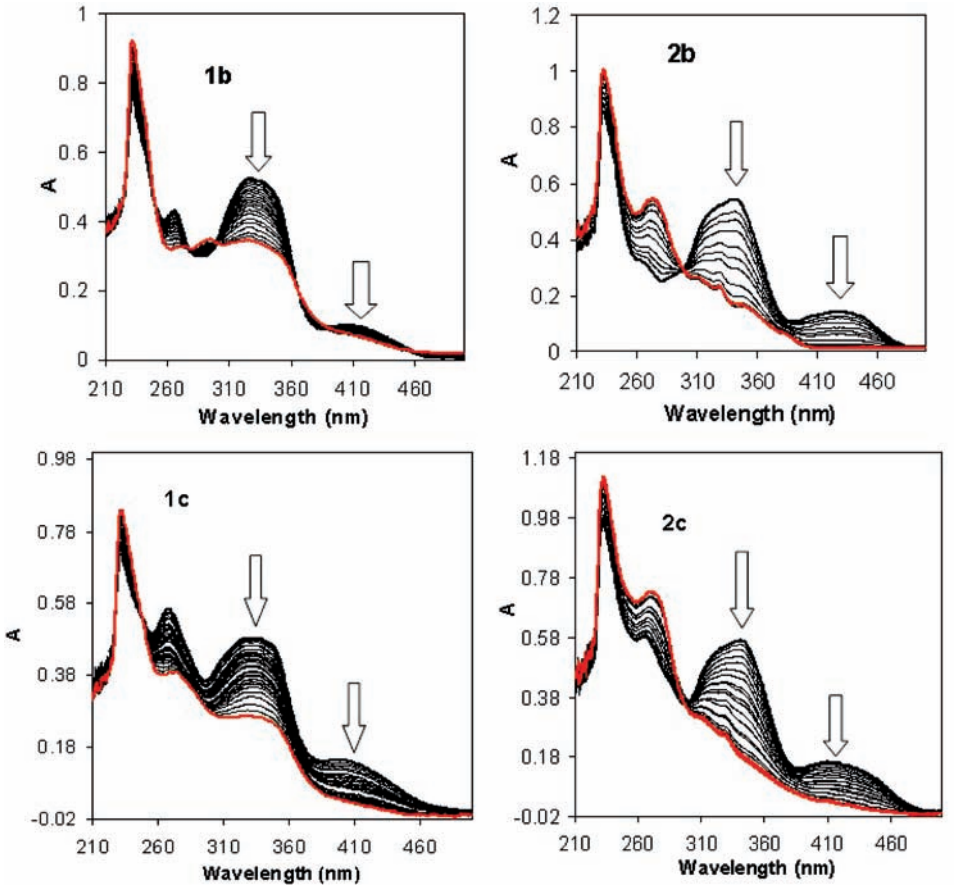

Figure 16. UV−vis spectral change of **1b** and **2b** (top, 2.0×10^{-5} M) and **1c** and **2c** (bottom, 1.0×10^{-5} M) with the addition of NBu_4F in CH_2Cl_2.

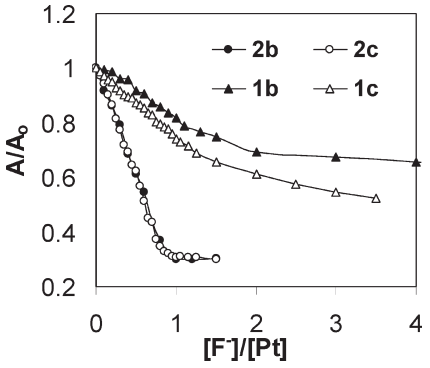

Figure 17. The plots of A/A_o vs $[F^-]/[Pt]$ at ~340 nm for **1b**, **2b**, **1c**, and **2c**.

The difference between the mononuclear Pt(II) py complex **2b** and the corresponding dinuclear bipy complex **2c** is that the amount of F^- needed to reach the saturation point for **2c** is about twice that for **2b** due to the presence of two boron acceptor centers. The plots of A/A_o versus equivalent $[F^-]$ per Pt atom at 345 nm (Figure 17) indicate that the two boron centers in **2c** respond to fluoride ions as they were two fully independent boron units with binding strengths identical to that of the mononuclear Pt(II) compound **2b**, thus supporting the position that there is little electronic communication between the two boron centers in the dinuclear Pt(II) complexes. This conclusion can also be reached by the essentially identical change of the UV−vis spectra of **2b** and **2c** with fluoride ions shown in Figure 16. In contrast, the UV−vis spectral change of **1b** and **1c** is notably different: for **1b**, several isosbestic points are present at 280−500 nm, while for **1c**, they are absent. Furthermore, the plots of A/A_o versus $[F^-]/[Pt]$ for **1b** and **1c** shown in Figure 17 do not overlap, with **1c** showing somewhat greater response toward F^-. On the basis of these data, we can conclude that some degree of electronic communication is present between the two boron centers in **1c**. The apparent lack of electronic communications between the two Pt(II) units in **2c** is clearly caused by the strong steric interactions, which is much reduced in **1c**, making electronic communications between the two Pt(II) units via the bipy bridge possible in **1c**.

Phosphorescent Titration. Due to the difficulty of carrying out phosphorescent titration in an oxygen-free environment, the phosphorescent titration experiments were performed for the py and the bipy complexes only. The phosphorescent data provide qualitative information concerning the impact of the fluoride ions on luminescence, but they are not accurate in terms of stoichiometry due to the difficulty of controlling concentrations when preparing and transporting the sample for each addition of fluoride in and out of a drybox. Nonetheless, the titration data shown in Figure 18 illustrate that the addition of fluoride shifts the emission peak to a shorter wavelength for both **1b** and **2b**, with the emission color changing from yellow-green to blue-green. The fluoride adduct emission spectrum ($\lambda_{max} = 489$ nm) of **2b** is similar to that of $Pt(ppy)L_2$ complexes reported by Tompson and

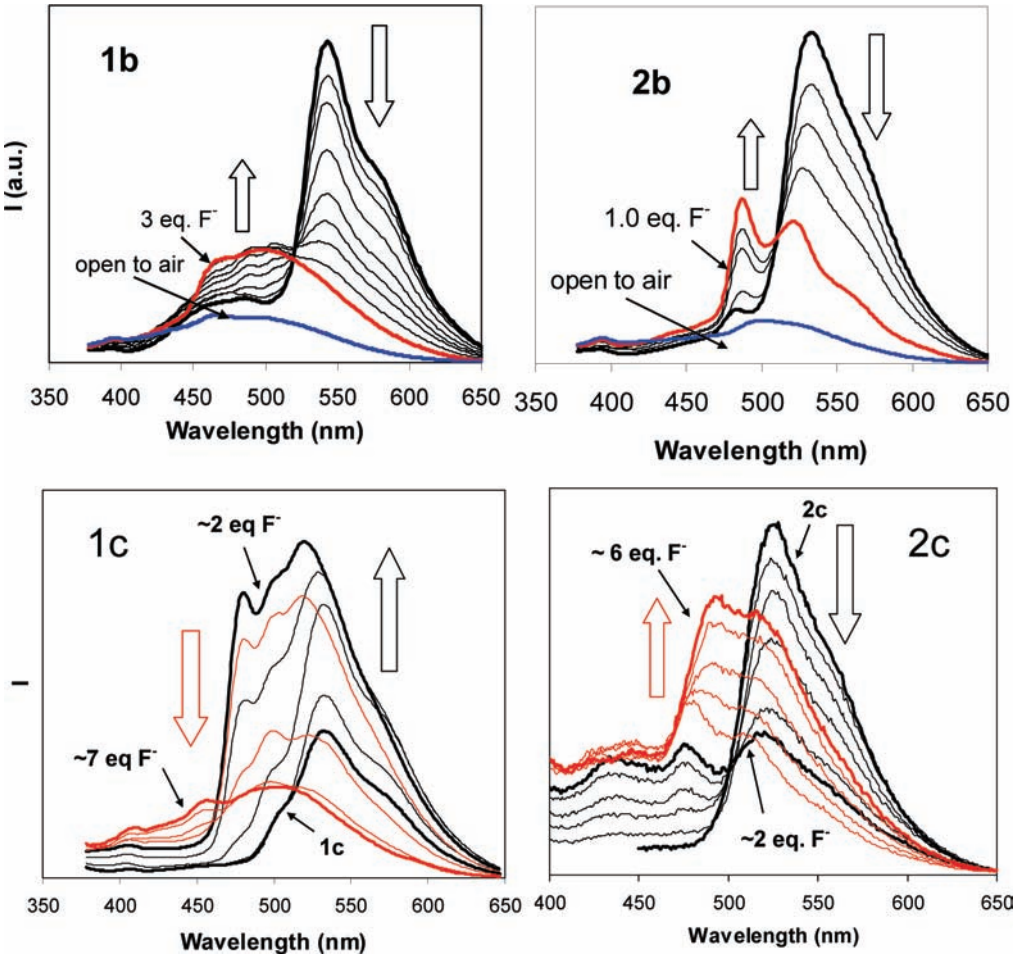

Figure 18. Phosphorescent emission spectral change of Pt(II) complexes **1b** and **2b** (top) and **1c** and **2c** (bottom) with the addition of NBu_4F in CH_2Cl_2 under N_2 at ambient temperature.

co-workers[9a] and is thus attributable to ppy-centered emission. The fluoride addition switches the ppy-B-based phosphorescence to ppy-based phosphorescence by blocking the boron center. The fluoride adduct spectrum of **1b** is more complex, with contributions not only from the ppy phosphorescence but also the ligand-based singlet emission band. Nevertheless, the general trend of the phosphorescent response of **1b** and **2b** toward fluoride ions is similar to that of the N,C-chelate complex[5h] Pt(*N*,*C*-BNPA)Ph(SMe_2), reported recently by us.

The phosphorescent titration spectra of the dinuclear complexes **1c** and **2c** display some unique features that are not observed in **1b** and **2b**. For **1c**, the emission spectrum initially gains intensity greatly with the addition of fluoride. Further addition of fluorides leads to the decrease of emission intensity, and the final emission spectrum of the fluoride adduct resembles that of the **1b** fluoride adduct, clearly due to the formation of the 2:1 adduct. The high-energy emission band with distinct vibrational features in the **1c** fluoride adduct is attributed to 4,4′-bipy (see 4,4′-bipy emission spectra in the Supporting Information). The initial rise of the emission intensity of **1c** with F^- may be explained by the formation of the 1:1 adduct which, if it behaves like **1b**, should have a much greater emission efficiency than **1c**, and thus, there should an enhancement of the emission. The fluoride ions may be therefore described as the "activator" for the emission of the 1:1 complex. This "activation" effect is only possible through electronic communication between the two Pt(II) units in the same molecule. The phosphorescent response of **1c** toward fluoride is therefore consistent with the UV−vis titration data.

In contrast to **1c**, which has a distinct emission spectral change for the 1:1 and 2:1 adducts, the spectral change of **2c** with fluoride resembles that of **2b**; namely, the original peak is quenched while the new ligand-centered emission peak at ~490 nm gains intensity. Compared to **2b**, there is an apparent two-stage change in the emission spectrum of **2c** with fluoride, which may be attributed to the 1:1 and 2:1 adducts. In addition, there is a high-energy emission band in the 400−480 nm region after the addition of ~2 equiv of fluorides in the spectrum of **2c**, which is not observed in the fluoride adduct of **2b** and is attributed to the 4,4′-bipy ligand. The phosphorescent titration results of **2c** indicate that the two Pt(II) units behave like two independent monomer units, which is consistent with the UV−vis titration data.

NMR Spectral Titration. To verify that the fluoride ions are indeed bound to the boron center in the metal complexes, we carried out NMR spectral titration experiments for all complexes. The ^1H NMR spectra of all complexes undergo gradual change with the addition of fluoride and become broad due to the equilibrium between bound and nonbound species (see Supporting

Table 5. ^{19}F NMR Data of the Fluoride Adducts for All Complexes

compound	**1a**	**1b**	**1c**	**2a**	**2b**	**2c**
^{19}F, ppm in CD_2Cl_2	−175.3	−175.8	−176.0	−176.9, −177.7	−177.1	−177.0

Chart 4

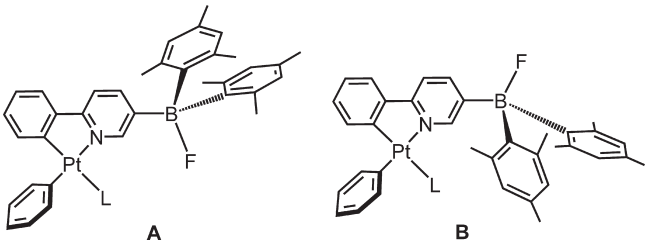

Information). ^{19}F NMR data (Table 5) are most informative. Our previous studies have shown that the chemical shift of F^- bound to a B(Ar)Mes_2 group appears typically at ∼−175 to −180 ppm. The ^{19}F NMR data indeed showed that all Pt(II) complexes except **2a** display one characteristic chemical shift at ∼−175 to −178 ppm that grows in intensity with an increasing amount of TBAF added (see Supporting Information), confirming that the fluoride is indeed bound to the boron center. The ^{19}F chemical shift of a fluoride bound to a Pt center usually appears in the region of −230 to −280 ppm, depending on the nature of other ligands and the oxidation state of the Pt atom with distinct $^1J_{Pt-F}$ coupling satellites.[20] The absence of any Pt−F signals in ^{19}F NMR spectra of all Pt(II) complexes further confirmed that the fluoride ion is bound to the boron center.

For the DMSO complex **2a**, two fluoride chemical shifts were observed at −176.9 ppm and −177.7 ppm with nearly equal intensity in the fluoride adducts, indicating the presence of isomers. The crystal structural data of previously published fluoride adducts involving a B(Ar)Mes_2 group[21] revealed that the two mesityl groups in the adduct are oriented above and below the B−Ar plane, respectively, to minimize steric interactions, and the F atom lies approximately in the same plane with B−Ar. As a consequence, if there is sufficient hindered rotation around the B−C(Ar) bond due to the bulky B(F)Mes_2 group, two possible and distinct structures for the fluoride adduct in the Pt(II) complexes can coexist in solution, as depicted for the *p*-ppy-B complex in Chart 4. For **2a**, the auxiliary ligand DMSO is on the same side as the B(F)Mes_2 group in the fluoride adduct and is much more sterically demanding than either phenyl or pyridyl, and perhaps as a consequence, both structures **A** and **B** are observed. For *p*-B-ppy complexes, the phenyl group is always on the same side as the $BMes_2$ group, which has a steric demand similar to that of py, and as a result, regardless of the nature of the auxiliary ligand L, only one ^{19}F chemical shift is observed.

(20) (a) Cross, R. J.; Haupt, M.; Rycroft, D. S.; Winfield, J. M. *J. Organomet. Chem.* **1999**, *587*, 195. (b) Jasim, S. A.; Perutz, R. N. *J. Am. Chem. Soc.* **2000**, *122*, 8685. (c) Clark, H. C. S.; Fawcett, J.; Holloway, J. H.; Hope, E. G.; Peck, L. A.; Russell, D. R. *Dalton Trans.* **1998**, 1249.

(21) Zhao, S. B.; Wucher, P.; Hudson, Z. M.; McCormick, T. M.; Liu, X. Y.; Wang, S.; Feng, X. D.; Lu, Z. H. *Organometallics* **2008**, *27*, 6446.

Conclusions

This study has shown that the two constitutional isomers of *p*-B-ppy and *p*-ppy-B have a distinct impact on the structures, stabilities, and electronic and photophysical properties of the Pt(II) complexes. For *p*-B-ppy, Pt(II) chelation does not alter the electron-accepting ability of B-ppy, compared to the free neutral ligand. The increased steric interactions in the Pt(II) complexes of *p*-B-ppy also significantly diminish the Lewis acidity of the B center, as demonstrated by the low binding strength of the Pt(II) complexes with fluorides, relative to the free *p*-B-ppy. For *p*-ppy-B, Pt(II) chelation does enhance its electron-accepting ability but does not significantly change its Lewis acidity with fluoride due to greater steric congestion in the complexes. Hence, we can conclude that, for N,C-chelate ligands, it is most effective with the boron moiety being directly conjugated with the nitrogen heterocycle in order to enhance the electron-accepting ability and Lewis acidity. The overall impact of metal chelation with N,C-chelate ligands on the electron-accepting ability and Lewis acidity of a triarylboron center is a balance of both electronic and steric factors. In the dinuclear Pt(II) complexes, weak electronic communication between the two boron centers is possible in sterically less congested systems such as **1c** due to the greater π-conjugation of the B(III) and Pt(II) centers with the 4,4′-bipy linker (which can rotate freely in solution in **1c**). Lastly, the phosphorescent decay lifetimes of the Pt(II) complexes *p*-B-ppy and *p*-ppy-B are all much longer than those of Pt(ppy)(acac) and its derivatives, which may be due to the stabilization of the excited state by the $BMes_2$ group or the influence of the phenyl ligand and the auxiliary ligand. To fully establish the role of the boron center in B-ppy and ppy-B ligands, it is necessary to synthesize Pt(*p*-B-ppy)(acac) and Pt(*p*-ppy-B)(acac) complexes so that direct comparison with Pt(ppy)(acac) can be made. This is currently being investigated in our laboratory and will be reported in due course.

Acknowledgment. We thank the Natural Sciences and Engineering Research Council of Canada for financial support and Dr. Rui-Yao Wang for his assistance in some of the crystal structural work.

Supporting Information Available: UV−vis and fluorescent titration spectra of *p*-ppy-B by TBAF; variable-temperature ^{1}H NMR data of **1c**; emission spectra of 4,4′-bipy in CH_2Cl_2; determination of binding constants with fluoride ions; complete ^{1}H NMR and ^{19}F NMR titration spectra of all Pt(II) complexes by TBAF; and complete crystal structural data of *p*-ppy-B, **1a**, **2a**, **1c**, and **2c**. This material is available free of charge via the Internet at http://pubs.acs.org.